Fitton, J.G., Mahoney, J.J., Wallace, P.J., and Saunders, A.D. (Eds.)
Proceedings of the Ocean Drilling Program, Scientific Results Volume 192

7. Relationships between Physical Properties and Alteration in Basement Rocks from the Ontong Java Plateau[1]

Xixi Zhao,[2] Maria Antretter,[3] Loren Kroenke,[4] Peter Riisager,[2, 5] and Stuart Hall[6]

ABSTRACT

In this manuscript, we present the results of a physical properties investigation carried out on basaltic cores recovered from the four Leg 192 basement sites, focusing on the relationship between physical properties and alteration in basalts. Variations in physical properties in the Leg 192 basement sites closely resemble each other and reflect the amount of alteration and vein formation in the basement basalts. *P*-wave velocities, magnetic susceptibilities, and densities for the dense massive basalts are higher than those of more altered and heavily veined basalts. Porosity-dependent alteration is observed at Leg 192 basement sites: *P*-wave velocity displays a general decrease with increasing loss on ignition and potassium content. These trends are consistent with trends documented for typical alteration of oceanic crust and suggest that basalt alteration is largely responsible for the variation of the physical properties exhibited by rocks at Leg 192 basement sites. Our physical property data support the conclusion that only low-temperature seawater-mediated alteration occurred in the lava flows of the Ontong Java Plateau (OJP). This lack of higher-temperature hydrothermal alteration is consistent with the idea that the OJP basement sites are far from their eruptive vents.

[1]Zhao, X., Antretter, M., Kroenke, L., Riisager, P., and Hall, S., 2004. Relationships between physical properties and alteration in basement rocks from the Ontong Java Plateau. *In* Fitton, J.G., Mahoney, J.J., Wallace, P.J., and Saunders, A.D. (Eds.), *Proc. ODP, Sci. Results,* 192, 1–33 [Online]. Available from World Wide Web: <http://www-odp.tamu.edu/publications/192_SR/VOLUME/CHAPTERS/109.PDF>. [Cited YYYY-MM-DD]
[2]Center for Study of Imaging and Dynamics of the Earth, Institute of Geophysics and Planetary Physics, University of California, Santa Cruz CA 95064, USA. Correspondence author: **xzhao@es.ucsc.edu**
[3]Institut für Geophysik, University of München, Theresienstrasse 41, D-80333 München, Germany.
[4]Institute of Geophysics, University of Hawaii, Honolulu HI 96822, USA.
[5]Danish Lithosphere Centre, Øster Voldgade 10, DK-1350 Copenhagen K, Denmark.
[6]Department of Geosciences, University of Houston, Houston TX 77204-5007, USA.

Initial receipt: 30 December 2003
Acceptance: 6 July 2004
Web publication: 14 September 2004
Ms 192SR-109

INTRODUCTION

The history of the Ontong Java Plateau (OJP) in the western Pacific, which is the largest oceanic large igneous province (LIP) in the world (Fig. F1), was investigated during Ocean Drilling Program (ODP) Leg 192. Understanding the origin and evolutionary history of the OJP is of particular importance because it is the best manifestation of mid-Cretaceous volcanism (~124–90 Ma) in the Pacific (Larson, 1991). Results from previous Deep Sea Drilling Project (DSDP) and ODP drilling expeditions to the OJP have shown that the OJP exhibits characteristics that are inconsistent with formation by mantle plume heads (e.g., Tarduno et al., 1991; Bercovici and Mahoney, 1994), a bolide impact (e.g., Rogers, 1982), or mantle avalanche (e.g., Muller, 2002). Other scientists (e.g., Ingle and Coffin, 2004) have recently argued that an extraterrestrial impact model is more consistent with existing data and suggested a large object (>10 km in diameter) may have struck the deep ocean basins and resulted in emplacement of the OJP. Despite the huge size of the OJP (larger than Alaska) and its potential role in contributing to our understanding of mantle circulation and environmental change in the past, the origin and evolution of the OJP is still poorly understood (Mahoney and Coffin, 1997).

Basement and sediment cores were recovered during Leg 192 at five widely spaced sites in previously unsampled areas of the OJP (Fig. F1). Four drill sites (1183, 1185, 1186, and 1187) successfully reached basaltic basement, which comprises a thick sequence of submarine pillow and massive lavas. The lava flows of the OJP have undergone low-temperature seawater-mediated alteration (Banerjee et al., 2004). Because responses to varying oceanographic conditions can result in changes in alteration regimes and in physical properties of the basalt, physical property parameters of the basaltic flows are useful for studying petrogenesis and environment of the OJP formation. Standard physical properties, such as *P*-wave velocity, density, porosity, magnetic susceptibility, and thermal conductivity, are useful indicators of alteration and can therefore be used to understand the relationship of physical properties to the alteration regime at the Leg 192 sites.

In this paper, we investigate the relationship between physical properties and alteration and vein formation in basaltic cores recovered from the four Leg 192 basement sites. We will first briefly mention the newly available age information about the basement sites and then outline the physical property data and explore their implications for understanding the interplay of primary volcanic emplacement and subsequent alteration.

LEG 192 BASEMENT SITES AND AGES

The site locations and alteration data are documented in detail in the site chapters of the Leg 192 *Initial Reports* volume (see Mahoney, Fitton, Wallace, et al., 2001) and relevant papers (Banerjee et al., 2004; **Banerjee and Honnorez,** this volume). Thus, we present only a simplified summary of the basement sites and their alteration characteristics in Table T1.

Recently completed whole-rock $^{40}Ar/^{39}Ar$ analyses on basaltic basement samples indicate that all Leg 192 basalts are ~120 Ma (Chambers et al., 2002, 2004), which is in excellent accordance with a Re-Os iso-

F1. Bathymetry map of the Ontong Java Plateau, p. 12.

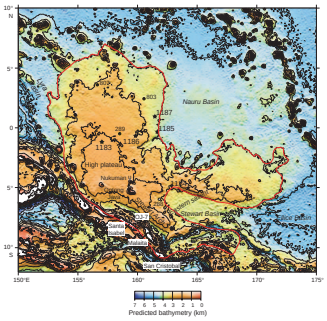

T1. Simplified hole summary, p. 21.

chron age of 121.5 ± 1.7 Ma derived from the basement sites (Parkinson et al., 2001). Using these constraints, it now appears that an immense part of the OJP may have formed in a single event at ~120 Ma. With the resolution of existing sampling and dating, the duration of this event could have been as short as 2 m.y. (Chambers et al., 2002). Shipboard and postcruise paleomagnetic studies for Leg 192 (Riisager et al., 2003, 2004) also suggest that the entire basalt sequence is normal magnetic polarity that is consistent with the Cretaceous Normal Superchron (120–84 Ma) and with the new ages of the rocks. The new ages of the OJP basement sites are also summarized in Table **T1.**

METHODS

On board the *JOIDES Resolution* we routinely measured sonic compressional (*P*-wave) velocities on cut samples. Moisture and density (MAD), including wet bulk density, grain density, dry bulk density, water content, void ratio, and porosity, were measured on discrete samples taken from each core recovered from Leg 192 sites. Magnetic susceptibility was also measured independently every 2 cm on the archive multisensor track (AMST) with the point-susceptibility meter, as well as on paleomagnetic minicores. Thermal conductivity was measured on selected split-rock samples from each core.

Measurements were made after cores had been allowed to stand for 2–4 hr to equilibrate to approximately ambient room temperature (i.e., 22°–24°C). All instruments and apparatuses used in the shipboard laboratory and the principles of the methods employed were described by Boyce (1976), ODP Shipboard Measurements Manual (Ocean Drilling Program, unpubl. data), American Society of Testing and Materials (ASTM, 1989), and Blum (1997). Shipboard MAD property measurements for Site 1187 were not completed because of the time constraints near the end of operation. As a partial remedy, additional measurements of MAD properties on several core intervals from Site 1187 were performed in the petrophysical laboratory at the First University of Naples (Italy) with a MultiVolume pycnometer 1305.

In order to examine the effects of alteration on the physical properties of Leg 192 basalts, the physical property data were compared with alteration and vein logs (**Banerjee and Honnorez,** this volume) of either the same samples used for physical property determination or samples adjacent to the physical property samples. This comparison is further supplemented with shipboard geochemical analyses of each site documented in Mahoney, Fitton, Wallace, et al. (2001).

PHYSICAL PROPERTY RESULTS

The "Physical Properties" sections in the site chapters of the Leg 192 *Initial Reports* volume present detailed accounts of shipboard physical property measurements. Complete tables and figures of physical property data for all Leg 192 sites are contained in Mahoney, Fitton, Wallace, et al. (2001). For this study, we use data points that were obtained from basement measurements only (Tables **T2, T3, T4, T5**). Several typos and errors from the previous published tables in Leg 192 *Initial Reports* volume were noticed and corrected in this study. Shore-based data points are included along with the figures of this paper.

T2. *P*-wave velocity, geochemical data, and vein logs, p. 22.

T3. MAD data, p. 29.

T4. Magnetic susceptibility data, p. 30.

T5. Thermal conductivity data, p. 33.

P-Wave Velocities

At all Leg 192 sites, a sharp velocity increase occurs at the boundary between sediments and basaltic basement (see "Physical Properties" sections in the site chapters in Mahoney, Fitton, Wallace, et al., 2001). As shown in Figure F2 and Table T2, *P*-wave velocities in the basement basalts of Hole 1183A are >5000 m/s (mean = 5508 m/s). A marked velocity low (4768 m/s) occurs at ~1140 meters below seafloor (mbsf), corresponding to a veined and fractured basalt (Sample 192-1183A-55R-3, 131–133 cm). This sample also has low bulk and grain densities (Fig. F2) and relatively high values of porosity, weight loss on ignition (LOI), and K_2O (Table T2).

Two holes were drilled at Site 1185. In the basement Units 1–5 of Hole 1185A, *P*-wave velocities range from 4641 to 5612 m/s (mean = 5122 m/s). In the basement units of Hole 1185B, *P*-wave velocities are lower (generally <5000 m/s) in Units 1, 4, 6, and 9, whereas velocities are typically >5000 m/s in Units 2, 3, and 10–12 (Fig. F3). The high *P*-wave velocities (>5000 m/s) in these relatively unveined basalts are associated with high bulk and grain densities and low porosity values (Fig. F3; Tables T2, T3).

Similarly, *P*-wave velocities in the basement units of Hole 1186A are typically >5000 m/s in the less veined basalt (e.g., Units 1, 2, and 4) and generally <5000 m/s in the more veined basalt (e.g., Unit 3) (Fig. F4; Table T2). The high *P*-wave velocities (>5000 m/s) in the relatively unveined basalts are once again associated with high bulk and grain densities and low porosity values (Fig. F4; Table T3). The transition from pillowed to massive basalt, observed in the core at 981 mbsf, is also apparent in the Formation MicroSanner (FMS) images. All logs correlate very closely with lithologic changes identified from core descriptions (Mahoney, Fitton, Wallace, et al., 2001).

For Site 1187, *P*-wave velocities are typically >5300 m/s in the relatively massive unveined basalt sections of Units 3, 5, 6, and 7 and generally <5300 m/s in the more abundantly veined basalt sections of these units, as well as in the remaining basement units (Fig. F5). The high *P*-wave velocities (>5300 m/s) measured in the relatively unveined basalt also correlate with the large magnetic susceptibility spikes observed in the same units. Below 500 mbsf, in the lower part of Unit 11 and through Unit 12, *P*-wave velocities decrease significantly (<5300 m/s), in similar fashion to mean bulk densities in this interval (Fig. F5).

Density and Porosity

Density and porosity are two of the most important variables controlling progressive alteration in the basalts (Carlson and Herrick, 1990). Little variation in grain density (2.9–3.1 g/cm³; mean = ~3.0 g/cm³) is present in basalts of basement from Site 1183 (Table T3). Porosity values are generally low (~3%) in the massive basalt but increase to 16% in veined basalt (Fig. F2).

In the basalts from Hole 1185B, bulk densities are higher (>2.4 g/cm³) within basement Units 2, 5, 10, and 11 and lower (<2.3 g/cm³) in Units 3 and 6–9. Both grain and bulk densities decrease downhole in Units 4–9, corresponding to a lithologic change from massive basalt to heavily veined basalt. Below Unit 9, an increase in bulk density correlates with a lithologic change from veined basalt back to massive basalt in Units 10–12 (Fig. F3). Porosity ranges from 16% to 4% in Hole 1185B, with high values in heavily veined basalt.

F2. Minicore measurements, Hole 1183A, p. 13.

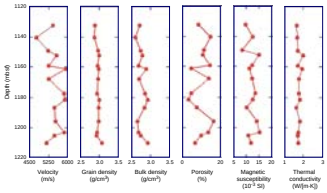

F3. Minicore measurements, Hole 1185B, p. 14.

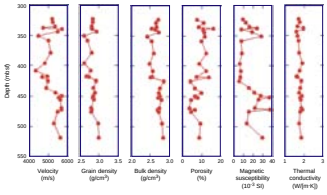

F4. Minicore measurements, Hole 1186A, p. 15.

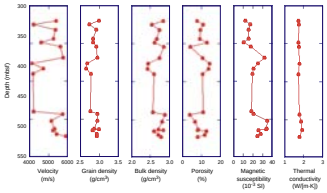

F5. Minicore measurements, Hole 1187A, p. 16.

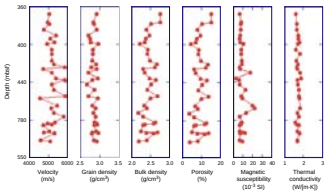

In general, both grain and bulk density decrease downhole in Unit 3 at Site 1186, corresponding to a lithologic change from massive basalt to heavily veined basalt. Below 966.85 mbsf, in the basalt of basement Unit 1, bulk density increases to an average of 2.7 g/cm^3. Bulk densities in basement Unit 3 are slightly lower than in other basement units. Below the top of Unit 4 (Section 192-1186A-36R-4), an increase in bulk density correlates with a change from the veined basalt back to massive basalt (Fig. F4). Similar to those at Sites 1183 and 1185, porosity ranges from 14% to 4% in the basalt of the basement units from Site 1186.

Shipboard petrological description suggests that the basalt in Hole 1187A underwent the greatest overall alteration of basement of any Leg 192 site (see "Alteration" in the "Site 1187" chapter in the Leg 192 *Initial Reports* volume; Shipboard Scientific Party, 2001). It is interesting to note, however, that MAD properties in the basement of Site 1187 are similar to those at other Leg 192 sites, with average grain and bulk densities at 2.8 g/cm^3 and 2.7 g/cm^3, respectively. Porosity ranges from 15% to 4% in the basalt of the basement units from Site 1187 (Fig. F5), also similar to those at other Leg 192 sites.

Magnetic Susceptibility

As shown in Figure F2 and Table T4, magnetic susceptibility values are, in general, quite uniform downhole at Site 1183. On a finer scale, however, dense massive basalt (e.g., Sample 192-1183A-57R-1, 131–133 cm; 1152 mbsf) always exhibited higher magnetic susceptibility than more altered and heavily veined basalt (e.g., Sample 192-1183A-56R-3, 118–120 cm; 1149.1 cm).

For Holes 1185A and 1185B, the peaks in magnetic susceptibility correlate well with the locations of massive basalt. For example, the magnetic susceptibility profile of basement units in Hole 1185B has two large spikes (>30 × 10^{-3} SI units) (Fig. F3); these spikes correspond to intervals of massive basalt without veins. On the other hand, heavily veined basalt in basement Units 6–9 exhibits much lower magnetic susceptibility values than the massive basalt both above and below these units (Tables T2, T4).

Similar features are seen in the magnetic susceptibility profile for Hole 1186A. We observed a distinct difference between the pillow lavas, with relatively low magnetic susceptibility, and the more massive lava flows, with high susceptibility (Fig. F4; Table T4).

We obtained similar results at Site 1187; higher magnetic susceptibility values (>12 × 10^{-3} SI units) for Site 1187 basement units correlate with the presence of massive basalt (Fig. F5), and the massive interiors of large pillows have slightly higher magnetic susceptibility than the more finely grained pillow margins. Downhole magnetic susceptibility values for Site 1187 are slightly but noticeably lower than those for Sites 1185 and 1186. This observation is probably consistent with the dominantly pillowed nature of the basalts recovered in this hole.

Thermal Conductivity

Thermal conductivity values of the basalts from Site 1183, commonly between 1.7 and 2.0 W/(m·K), exhibit little scatter in the depth interval from 1130.3 to 1210.0 mbsf (Fig. F2; Table T5).

Thermal conductivity in basement units from Hole 1185B slightly increases with depth (Fig. F3; Table T5). The average thermal conductivity for the basement units is 1.8 W/(m·K). The maximum and minimum

values (at ~340 and ~415 mbsf, respectively) (see Fig. F3; Table T5) correspond to relatively dense massive gray basalt in Section 192-1185B-6R-5 and yellowish brown basalt in Section 15R-1, respectively (see Mahoney, Fitton, Wallace, et al., 2001).

In the basalt from the basement units of Site 1186, thermal conductivity remains fairly constant downhole (Fig. F4; Table T5). The average thermal conductivity for the basement units is 1.8 W/(m·K), the same as the basement basalt at Site 1185.

Thermal conductivity values at Site 1187 vary from 1.6 to 1.9 W/(m·K), with slightly higher values in the dense massive basalt and slightly lower values in the more altered and veined basalt (Tables T2, T5). The average thermal conductivity of the basalt is 1.7 W/(m·K), similar to basalt from Site 1186. A progressive increase in thermal conductivity with increasing hydrothermal alteration of basalts has been observed from studies of deep drill holes in Iceland and Bermuda (Oxburgh and Agrell, 1982; Hyndman et al., 1979). This pattern of variation is apparently not evident for the Site 1187 basalts.

Crossplots

Figure F6 shows *P*-wave velocity plotted against bulk density and porosity for Leg 192 basement sites. For Sites 1183, 1185, and 1186, the velocity-bulk density plots show an expected positive correlation routinely noted for DSDP and ODP basalt sites (e.g., Christensen and Salisbury, 1972; Busch et al., 1992). However, no such relationship was apparent between velocity and bulk density data for Site 1187. The same is true with the velocity vs. porosity crossplots; whereas other sites show an expected trend such as by the Wyllie et al. (1956) equation

$$V^{-1} = (1 - \phi)/V_{ma} + \phi/V_f,$$

where

- V = whole-rock compressional wave velocity,
- ϕ = fractional porosity,
- V_{ma} = matrix velocity, and
- V_f = pore fluid velocity, with negative correlation between porosity and velocity,

no obvious relationship was found on the velocity-porosity crossplot for Site 1187. Jarrard et al. (2003) point out that the Wyllie et al. (1956) equation is only an empirical approximation because theoretical equations (e.g., Gassmann, 1951) require elastic moduli that are rarely measured. Matrix velocities for basalts vary because of changes in alteration and composition (Serra, 1986).

Velocity-magnetic susceptibility crossplots are used to establish the relationship between the two physical parameters. Despite the large intrasite variations, an overall correlation between velocity and magnetic susceptibility is observed (Fig. F7). For the most part, higher velocity values correspond to higher magnetic susceptibilities. On the other hand, grain density vs. magnetic susceptibility crossplots show significant scatter and a complicated relationship that we cannot interpret with confidence (Fig. F8). Although the differences in magnetic susceptibility have several single or combined reasons (e.g., type of magnetic mineralogy, concentration, grain size and shape, etc.), they may be potentially helpful in examining the question of rock alteration.

F6. *P*-wave velocity and bulk density and porosity, p. 17.

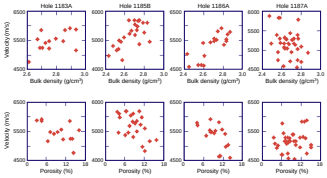

F7. *P*-wave velocity and magnetic susceptibility, p. 18.

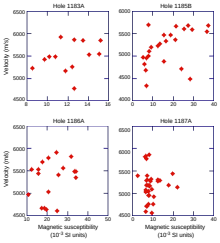

F8. Grain density and magnetic susceptibility, p. 19.

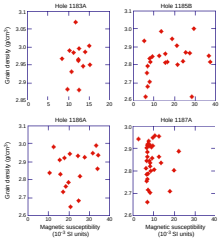

Crossplots of thermal conductivity vs. grain density do not reveal any obvious relationships (Fig. F9). This may reflect the fact that thermal conductivity measurements for all Leg 192 sites generally show only minor fluctuations downhole.

F9. Thermal conductivity and grain density, p. 20.

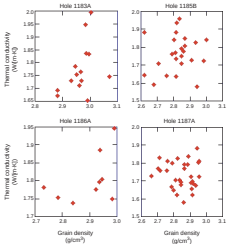

DISCUSSION

Because of the lack of detailed biostratigraphy and magnetostratigraphy to provide control points for depth-age conversion for Leg 192 basement holes, we are unable to convert data from depth domain to time domain to make intersite comparisons of physical properties. Nevertheless, we notice that variations in physical properties within the basement units at Leg 192 sites closely resemble each other, despite the geographically widespread locations of the drill sites. Results of anisotropy of magnetic susceptibility measurements from both pillowed and more massive basalt units from Leg 192 basement sites indicate broad similarities in their general properties (Hall et al., 2004). These observations appear to be consistent with the hypotheses that low-temperature alteration of oceanic basalts mostly occurred during or immediately after initial cooling (Kent and Gee, 1996) and crustal alteration is negligible beyond 10 Ma (Carlson, 1998). Our physical property data confirm the petrological, mineralogical, and geochemical evidence that basalts from all Leg 192 sites show similar effects of alteration, resulting in the development of various veins (Banerjee et al., 2004) (see Table T1). The absence of much alteration and of sedimentary interbeds in the deeper portion of recovered sections favor the hypothesis that lava emplacement on the OJP lasted only a short period of time (Berger et al., 1991).

An interesting result of the shipboard physical property study is that no significant velocity anisotropy was observed at Leg 192 sites (see tables in the "Physical Properties" sections in the site chapters of Mahoney, Fitton, Wallace, et al., 2001), which indicates that tectonically induced lateral compression may be negligible. This would suggest that alteration is variable—mainly vertical—within the site, with little horizontal alteration. What appears clear from this study is that physical properties at Leg 192 sites reflect the amount of alteration and vein formation in the basement basalts. Dense massive basalts always exhibit higher *P*-wave velocities, magnetic susceptibilities, and densities than the more altered and heavily veined basalts. Alteration indicators, such as potassium content (K_2O) and LOI data, also suggest that the degree of alteration decreases within the massive basalts at Leg 192 sites (Mahoney, Fitton, Wallace, et al., 2001). Porosity-dependent alteration is seen at Leg 192 basement sites: *P*-wave velocity generally decreases with increasing LOI and potassium content. These trends are consistent with trends documented for typical alteration of oceanic crust and suggest the alteration is largely responsible for the variation of the physical properties exhibited by basalts at Leg 192 basement sites. Many studies have provided comprehensive reviews of low-temperature alteration processes (e.g., Honnorez, 1981; Thompson, 1991; Jarrad et al., 2003). Fractures and veins represent the most important pathways that allow significant penetration of fluids into the rock and control alteration. Alteration would enhance fluid flow and increase porosity. High porosity would in turn promote alteration because of high permeability (Jarrad et al., 2003). Alteration would also replace primary, high-density phases (such as olivine, clinopyroxene, and plagioclase) with secondary, low-density phases (such as clay minerals) and thus decrease *P*-wave veloc-

ity. This observed pattern at Leg 192 basement sites is, however, opposite to the prediction of the standard model for aging of oceanic crust (e.g., Jacobson, 1992), which suggests that alteration minerals eventually fill cracks and voids, thereby reducing porosity and increasing *P*-wave velocity.

Data on hydrothermal activity are critical for understanding the oceanographic and climatic effects of plateau formation. Leg 192 OJP basement sites show almost no evidence of anything but low-temperature (less than ~100°C) seawater-mediated alteration in either the lava flows or overlying sediments (e.g., Babbs, 1997; Banerjee et al., 2004). Our physical property data also support this conclusion. This lack of higher-temperature hydrothermal alteration is consistent with the idea that the OJP basement sites are presumably far from their eruptive vents. Major hydrothermal systems would be expected to be centered around major eruptive loci (Tejada et al., 1996). The fact that types and amounts of alteration at all of the basement sites are similar to each other is in turn consistent with the observation that OJP drill sites are relatively unaffected by volcanism and deformation associated with the collision of the plateau and the north Solomon subduction zone in late Oligocene time (Kroenke et al., 1986; Riisager et al., 2003).

CONCLUSIONS

Based on physical property results obtained during our study of Leg 192 cores, we can draw the following conclusions.

The physical property data obtained from Leg 192 basement sites exhibit changes that reflect the amount of alteration and vein formation in the basement basalts. *P*-wave velocities, magnetic susceptibilities, and densities for the dense massive basalts are higher than those of more altered and heavily veined basalts. These trends are consistent with trends documented for typical alteration of oceanic crust and suggest the basalt alteration is largely responsible for the variation of the physical properties exhibited by igneous rocks at Leg 192 basement sites. Our physical property data support the conclusion that only low-temperature seawater-mediated alteration occurred in the lava flows of the OJP. This lack of higher-temperature hydrothermal alteration is consistent with the idea that the OJP basement sites are far from their eruptive vents.

This study has demonstrated that physical property studies on core samples can provide important information that has considerable relevance to understanding the evolution of the OJP.

ACKNOWLEDGMENTS

We are indebted to Mario Iorio and Alessio Langella of the petrophysical laboratory at the First University of Naples, Italy, for their great assistance. We thank Roy Wilkens, Neil Banerjee, and Paul Wallace for insightful comments and constructive suggestions that substantially improved this manuscript. This research used samples and/or data provided by the Ocean Drilling Program (ODP). ODP is sponsored by the U.S. National Science Foundation (NSF) and participating countries under management of Joint Oceanographic Institutions (JOI), Inc. Funding for this research was provided by U.S. Science Support Program and NSF grants EAR 443549-22178 and EAR 443747-22250 to X. Zhao, the

Danish National Research Foundation to P. Riisager, U.S. Science Support Program to S. Hall, and ODP/Germany project number So 72/70-1 to M. Antretter. Funding was also provided by the Center for the Study of Imaging and Dynamics of the Earth, Institute of Geophysics and Planetary Physics at the University of California, Santa Cruz, contribution number 468. The authors acknowledge the invaluable assistance and skill provided by all of the Leg 192 shipboard scientists, the ODP marine technicians, and the crew of the *JOIDES Resolution*. We also wish to express our appreciation to the shore-based ODP staff for all of their precruise and postcruise efforts.

REFERENCES

ASTM, 1989. *Annual Book of ASTM Standards for Soil and Rock: Building Stones* (Vol. 4.08): *Geotextiles:* Philadelphia (Am. Soc. Testing and Mater.).

Babbs, T.L., 1997. Geochemical and petrological investigations of the deeper portions of the Ontong Java Plateau: Malaita, Solomon Islands [Ph.D. dissert.]. Leicester Univ., UK.

Banerjee, N.R., Honnorez, J., and Muehlenbachs, K., 2004. Low-temperature alteration of submarine basalts from the Ontong Java Plateau. *In* Fitton, J.G., Mahoney, J.J., Wallace, P.J., and Saunders, A.D. (Eds.), *Origin and Evolution of the Ontong Java Plateau.* Geol. Soc. Spec. Publ., 229:259–273.

Bercovici, D., and Mahoney, J., 1994. Double flood basalts and plume head separation at the 660-km discontinuity. *Science,* 266:1367–1369.

Berger, W.H., Kroenke, L.W., Mayer, L.A., and Shipboard Scientific Party, 1991. Ontong Java Plateau, Leg 130: synopsis of major drilling results. *In* Kroenke, L.W., Berger, W.H., Janecek, T.R., et al., *Proc. ODP, Init. Repts.,* 130: College Station, TX (Ocean Drilling Program), 497–537.

Blum, P., 1997. Physical properties handbook: a guide to the shipboard measurement of physical properties of deep-sea cores. *ODP Tech. Note,* 26 [Online]. Available from World Wide Web: <http://www-odp.tamu.edu/publications/tnotes/tn26/INDEX.HTM>. [Cited 2001-09-02]

Boyce, R.E., 1976. Definitions and laboratory techniques of compressional sound velocity parameters and wet-water content, wet-bulk density, and porosity parameters by gravimetric and gamma-ray attenuation techniques. *In* Schlanger, S.O., Jackson, E.D., et al., *Init. Repts. DSDP,* 33: Washington (U.S. Govt. Printing Office), 931–958.

Busch, W.H., Castillo, P.R., Floyd, P.A., and Cameron, G., 1992. Effects of alteration of physical properties of basalts from the Pigafetta and East Mariana basins. *In* Larson, R.L., Lancelot, Y., et al., *Proc. ODP, Sci. Results,* 129: College Station, TX (Ocean Drilling Program), 485–499.

Carlson, R.L., 1998. Seismic velocities in the uppermost oceanic crust: age dependence and the fate of Layer 2A. *J. Geophys. Res.,* 103:7069–7077.

Carlson, R.L., and Herrick, C.N., 1990. Densities and porosities in the oceanic crust and their variations with depth and age. *J. Geophys. Res.,* 95:9153–9170.

Chambers, L.M., Pringle, M.S., and Fitton, J.G., 2004. Phreatomagmatic eruptions on the Ontong Java Plateau: an Aptian $^{40}Ar/^{39}Ar$ age for volcaniclastic rocks at ODP Site 1184. *In* Fitton, J.G., Mahoney, J.J., Wallace, P.J., and Saunders, A.D. (Eds.), *Origin and Evolution of the Ontong Java Plateau.* Geol. Soc. Spec. Publ., 229:325–331.

Chambers, L.M., Pringle, M.S., and Fitton, J.G., 2002. Age and duration of magmatism on the Ontong Java Plateau: $^{40}Ar/^{39}Ar$ results from ODP Leg 192. *Eos, Trans. Am. Geophys. Union,* 83 (Suppl.):V71B-1271. (Abstract)

Christensen, N.I., and Salisbury, M.H., 1972. Sea floor spreading, progressive alteration of Layer 2 basalts, and associated changes in seismic velocities. *Earth Planet. Sci. Lett.,* 15:367–375.

Gassmann, F., 1951. Elastic waves through a packing of spheres. *Geophysics,* 15:673–685.

Honnorez, J., 1981. The aging of the oceanic crust at low temperature. *In* Emiliani, C. (Ed.), *The Sea* (Vol. 7): *The Oceanic Lithosphere:* New York (Wiley), 525–587.

Hyndman, R.D., Christensen, N.I., and Drury, M.J., 1979. Seismic velocities, densities, electrical resistivities, porosities and thermal conductivities of core samples from boreholes into the islands of Bermuda and the Azores. *In* Talwani, M., Harrison, C.G., and Hayes, D.E. (Eds.), *Deep Drilling Results in the Atlantic Ocean: Ocean Crust.* Am. Geophys. Union, Maurice Ewing Ser., 2:94–112.

Ingle, S., and Coffin, M., 2004. Impact origin of the greater Ontong Java Plateau? *Earth Planet. Sci. Lett.,* 218:123–134.

Jacobson, R.S., 1992. The impact of crustal evolution on changes of the seismic properties of the uppermost ocean crust. *Rev. Geophys.,* 30:23–42.

Jarrard, R.D., Abrams, L.J., Pockalny, R., and Larson, R.L., 2003. Physical properties of upper oceanic crust: Ocean Drilling Program Hole 801C and the waning of hydrothermal circulation. *J. Geophys. Res.,* 108:10.1029/2001JB001727.

Kent, D.V., and Gee, J., 1996. Magnetic alteration of zero-age oceanic basalt. *Geology,* 24:703–706.

Kroenke, L.W., Resig, J., and Cooper, P.A., 1986. Tectonics of the southeastern Solomon Islands: formation of the Malaita Anticlinorium. *In* Vedder, J.J., and Tiffin, D.L. (Eds.), *Geology and Offshore Resources of Pacific Island Arcs, Solomon Islands Region.* Earth Sci. Ser. (NY), 4:109–116.

Larson, R.L., 1991. Latest pulse of Earth: evidence for a mid-Cretaceous super plume. *Geology,* 19:547–550.

Mahoney, J.J., and Coffin, M.F. (Eds.), 1997. *Large Igneous Provinces: Continental, Oceanic, and Planetary Flood Volcanism.* Geophys. Monogr., 100.

Mahoney, J.J., Fitton, J.G., Wallace, P.J., et al., 2001. *Proc. ODP, Init. Repts.,* 192 [CD-ROM]. Available from: Ocean Drilling Program, Texas A&M University, College Station TX 77845-9547 USA.

Muller, R.A., 2002. Avalanches at the core-mantle boundary. *Geophys. Res. Lett.,* 29:10.1029/2002GL015938.

Oxburgh, E.R., and Agrell, S.O., 1982. Thermal conductivity and temperature structure of the Reydarfjordur borehole. *J. Geophys. Res.,* 87:6423–6428.

Parkinson, I.J., Schaefer, B.F., and ODP Leg 192 Shipboard Scientific Party, 2001. A lower mantle origin for the world's biggest LIP? A high precision Os isotope isochron from Ontong Java Plateau basalts drilled on ODP Leg 192. *Eos, Trans. Am. Geophys. Union,* 82:1398.

Riisager, P., Hall, S., Antretter, M., and Zhao, X.X., 2003. Paleomagnetic paleolatitude of Early Cretaceous Ontong Java Plateau basalts: implications for Pacific Apparent and True Polar Wander. *Earth Planet. Sci. Lett.,* 208:235–252.

Riisager, P., Hall, S., Antretter, M., and Zhao, X., 2004. Early Cretaceous Pacific palaeomagnetic pole from Ontong Java Plateau basement rocks. *In* Fitton, J.G., Mahoney, J.J., Wallace, P.J., and Saunders, A.D. (Eds.), *Origin and Evolution of the Ontong Java Plateau.* Geol. Soc. Spec. Publ., 229:31–44.

Rogers, G.C., 1982. Oceanic plateaus as meteorite impact signatures. Nature, 299:341–342.

Serra, O., 1986. *Fundamentals of Well-Log Interpretation* (Vol. 2): *The Interpretation of Logging Data.* Dev. Pet. Sci., 15B.

Shipboard Scientific Party, 2001. Site 1187. *In* Mahoney, J.J., Fitton, J.G., Wallace, P.J., et al., *Proc. ODP, Init. Repts.,* 192, 1–66 [CD-ROM]. Available from: Ocean Drilling Program, Texas A&M University, College Station TX 77845-9547, USA.

Tarduno, J.A., Sliter, W.V., Kroenke, L., Leckie, M., Mayer, H., Mahoney, J.J., Musgrave, R., Storey, M., and Winterer, E.L., 1991. Rapid formation of Ontong Java Plateau by Aptian mantle plume volcanism. *Science,* 254:399–403.

Tejada, M.L.G., Mahoney, J.J., Duncan, R.A., and Hawkins, M.P., 1996. Age and geochemistry of basement and alkalic rocks of Malaita and Santa Isabel, Solomon Islands, southern margin of the Ontong Java Plateau. *J. Petrol.,* 37:361–394.

Thompson, G., 1991. Metamorphic and hydrothermal processes: basalt-seawater interaction. *In* Floyd, P.A. (Ed.), *Oceanic Basalts:* New York (Van Nostrand Reinhold), 148–173.

Wyllie, M.R.J., Gregory, A.R., and Gardner, G.H.F., 1956. Elastic wave velocities in heterogeneous and porous media. *Geophysics,* 21:41–70.

Figure F1. Bathymetry map of the Ontong Java Plateau showing the locations of sites (stars) drilled on Leg 192 (after Mahoney, Fitton, Wallace, et al. 2001). The plateau is outlined. Previous ODP and DSDP drill sites are shown by black and white dots.

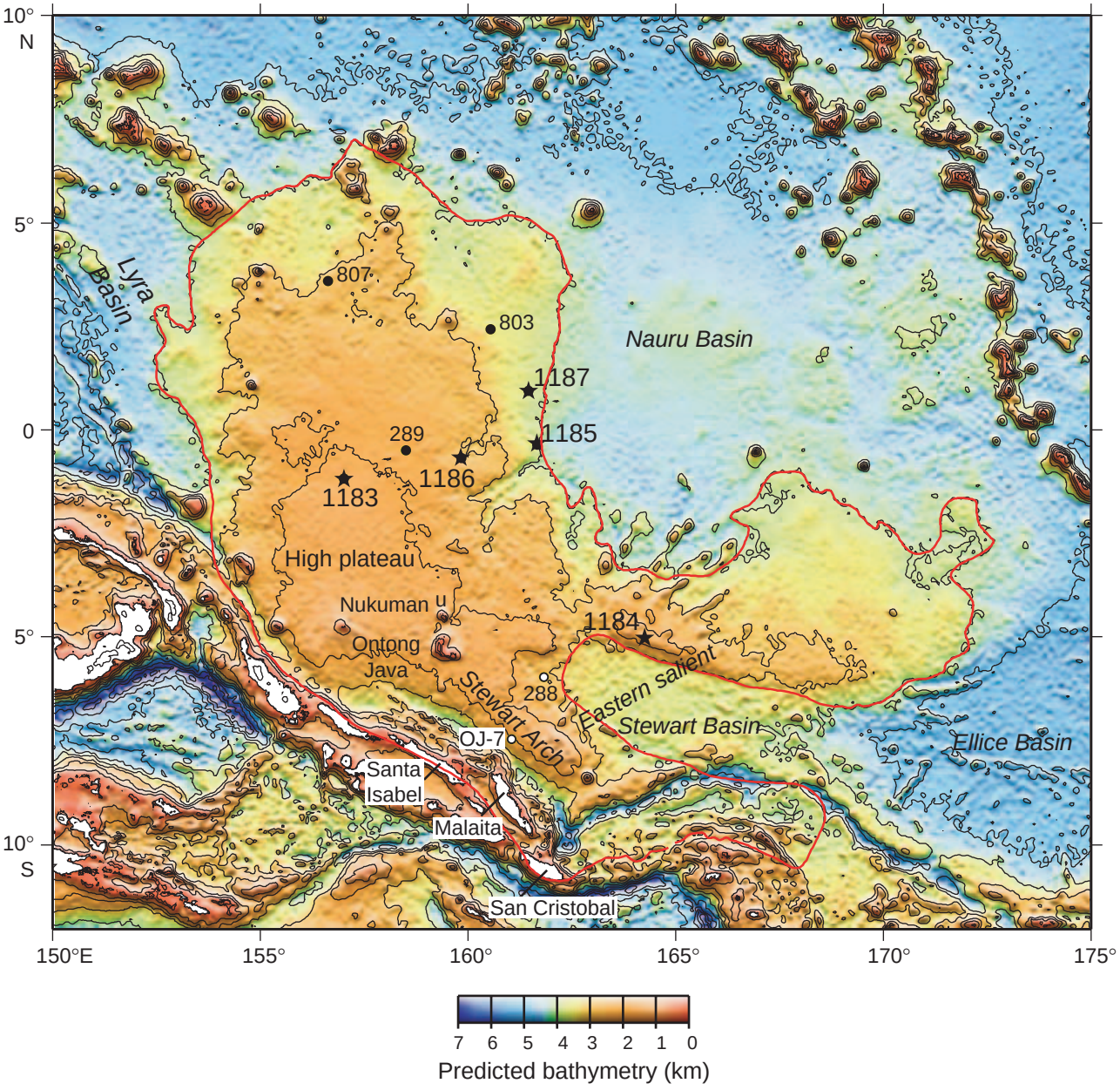

Figure F2. Minicore measurements of *P*-wave velocity, grain and bulk densities, porosity, magnetic susceptibility, and thermal conductivity vs. depth for Hole 1183A basement.

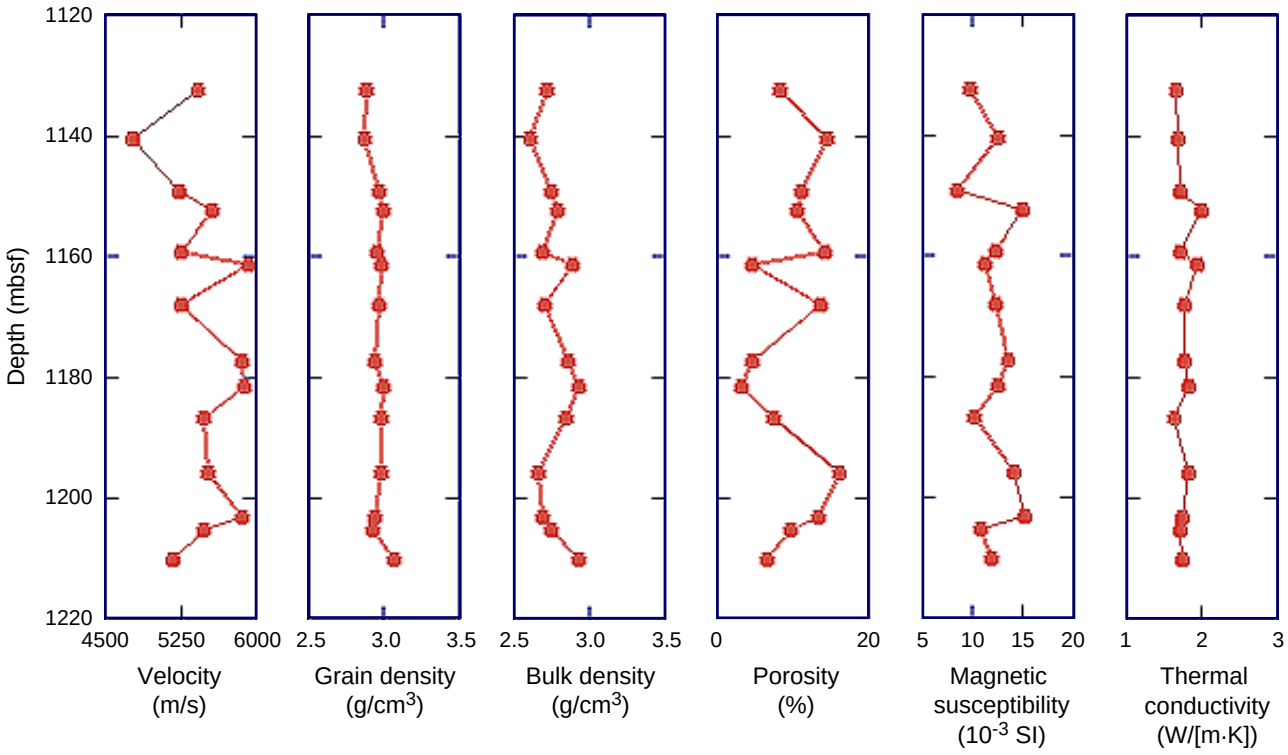

Figure F3. Minicore measurements of *P*-wave velocity, grain and bulk densities, porosity, magnetic susceptibility, and thermal conductivity vs. depth for Hole 1185B basement.

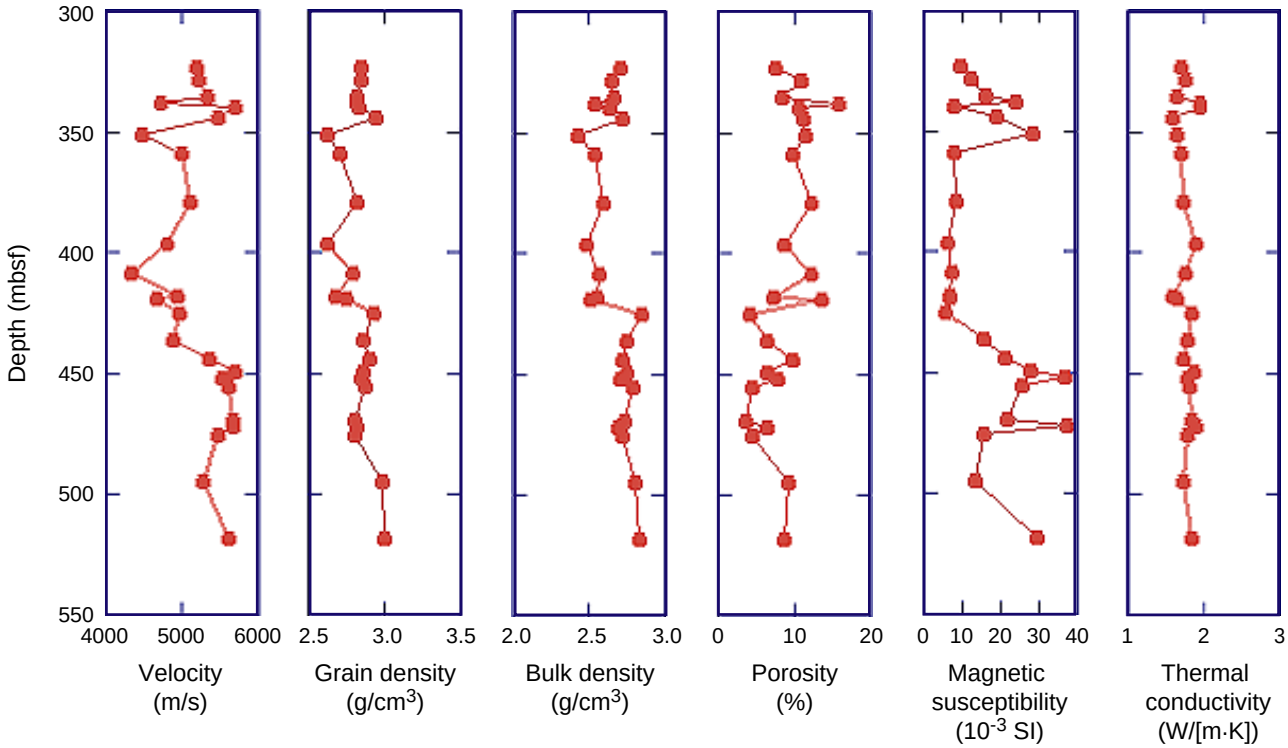

Figure F4. Minicore measurements of *P*-wave velocity, grain and bulk densities, porosity, magnetic susceptibility, and thermal conductivity vs. depth for Hole 1186A basement.

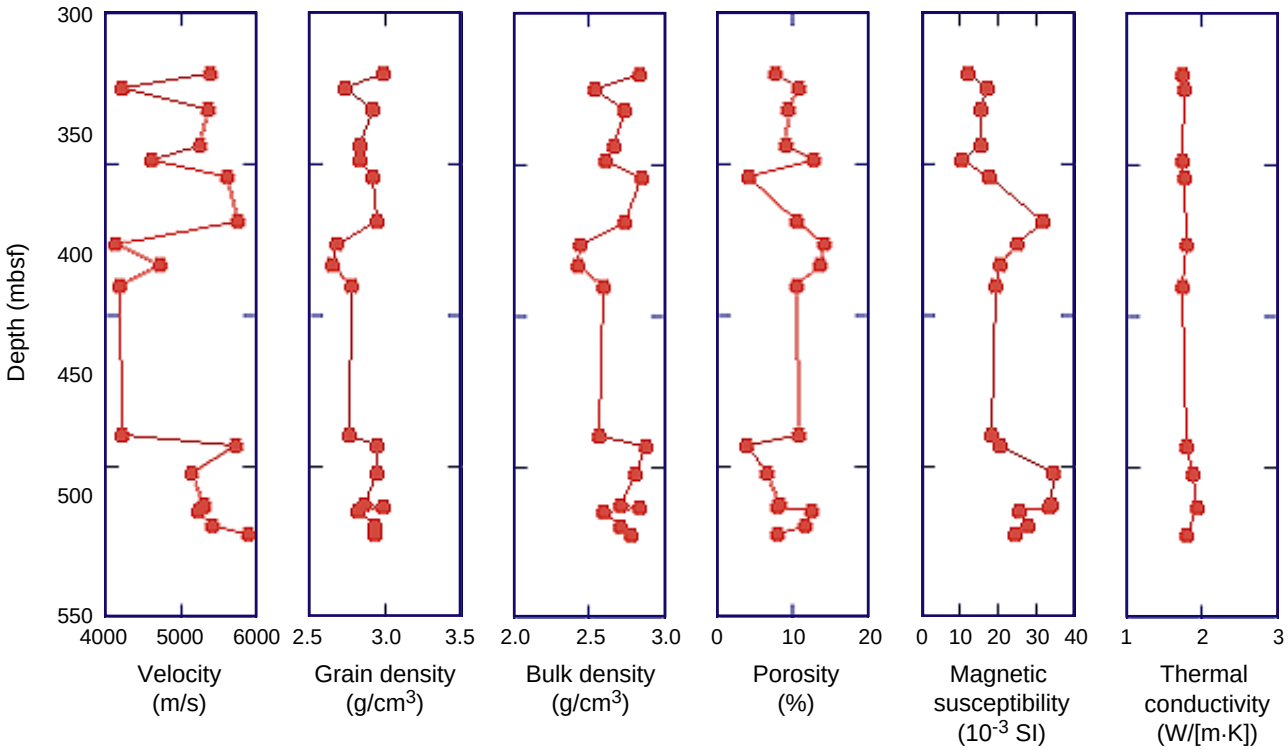

Figure F5. Minicore measurements of *P*-wave velocity, grain and bulk densities, porosity, magnetic susceptibility, and thermal conductivity vs. depth for Hole 1187A basement.

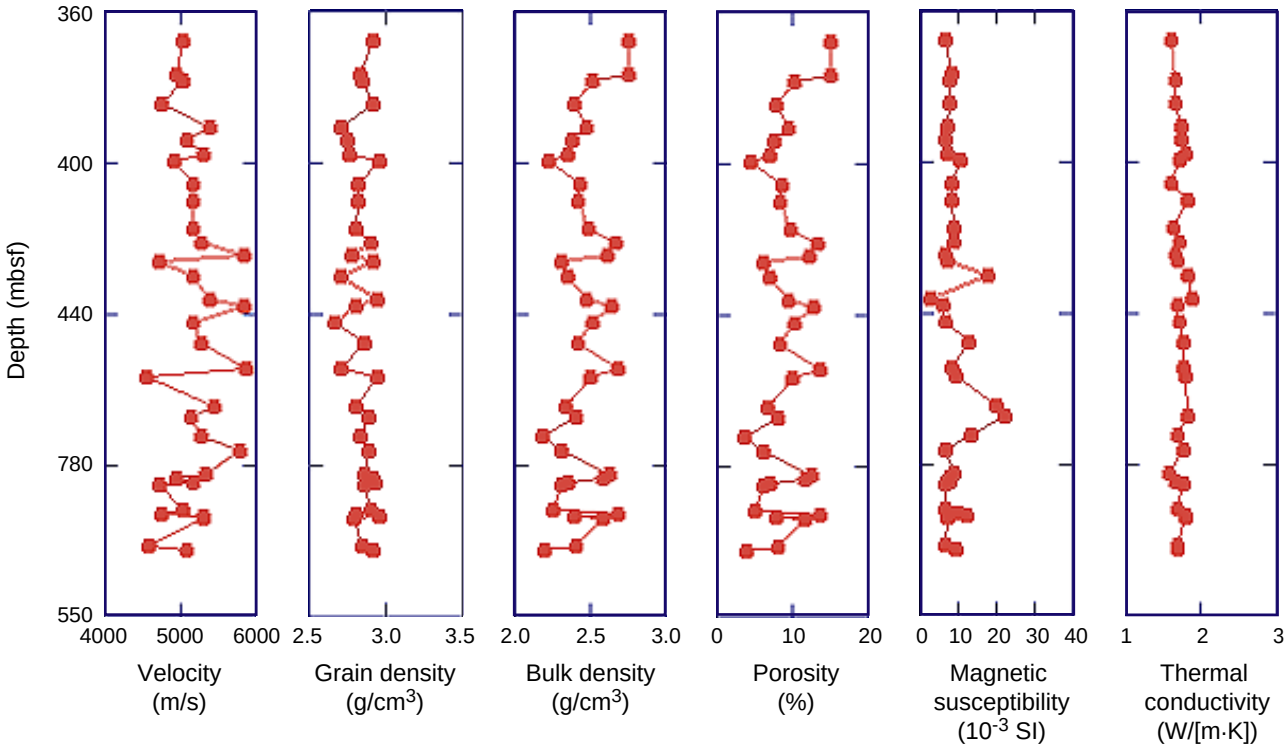

Figure F6. Crossplots of *P*-wave velocity and bulk density and porosity for Leg 192 basement sites.

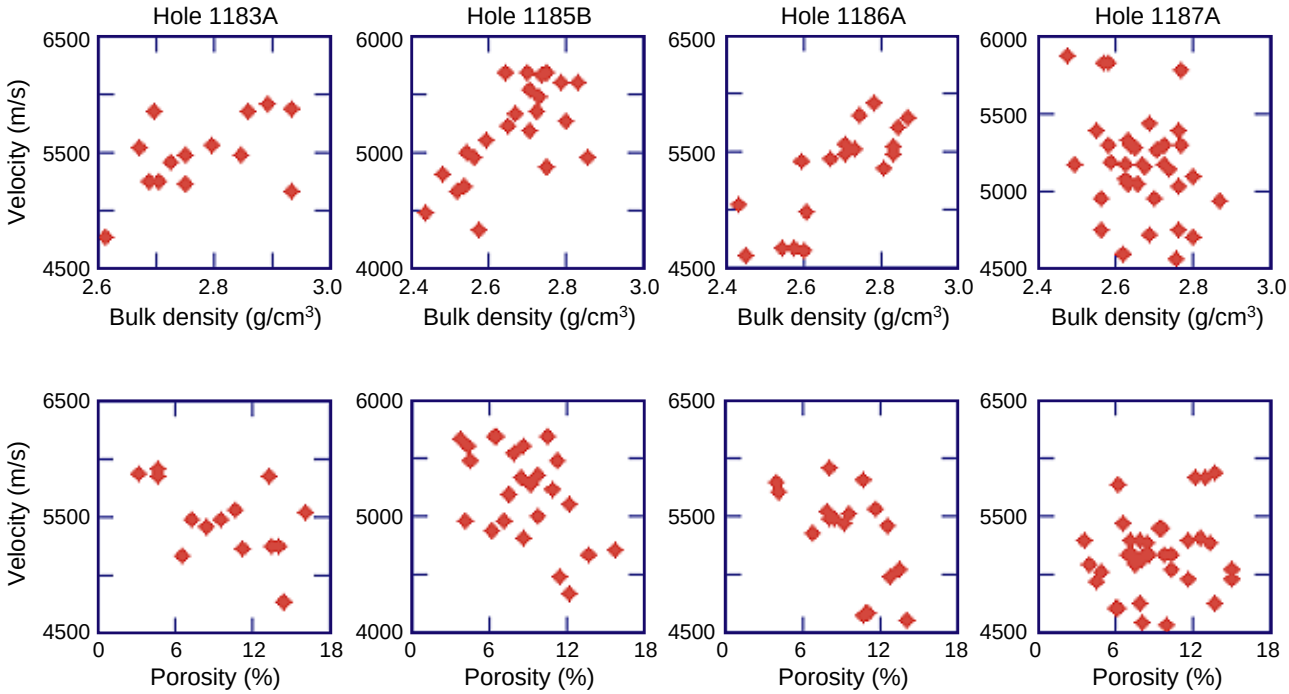

Figure F7. Crossplots of *P*-wave velocity and magnetic susceptibility for Leg 192 basement sites.

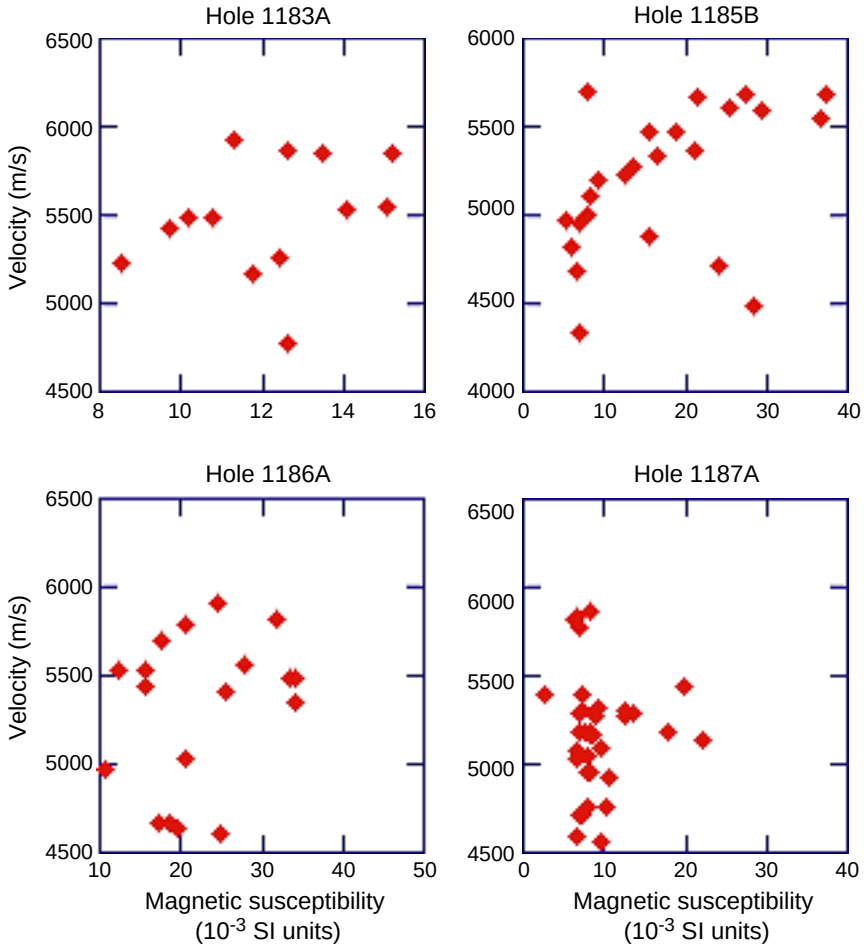

Figure F8. Crossplots of grain density and magnetic susceptibility for Leg 192 basement sites.

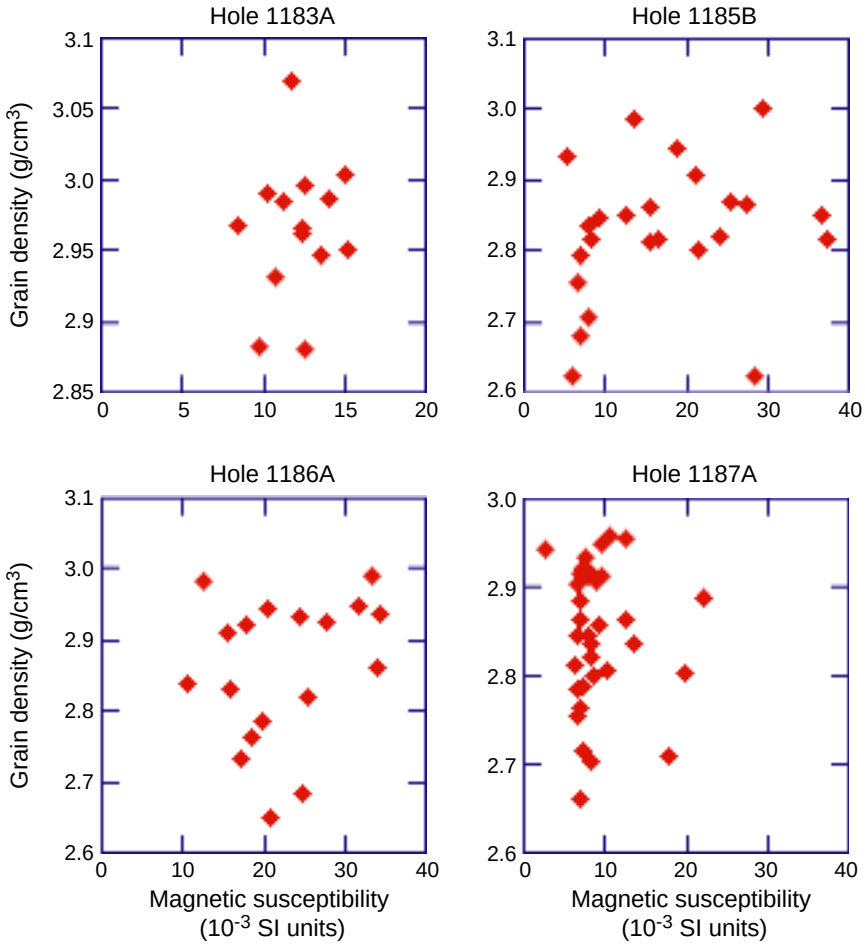

Figure F9. Crossplots of thermal conductivity and grain density for Leg 192 basement sites.

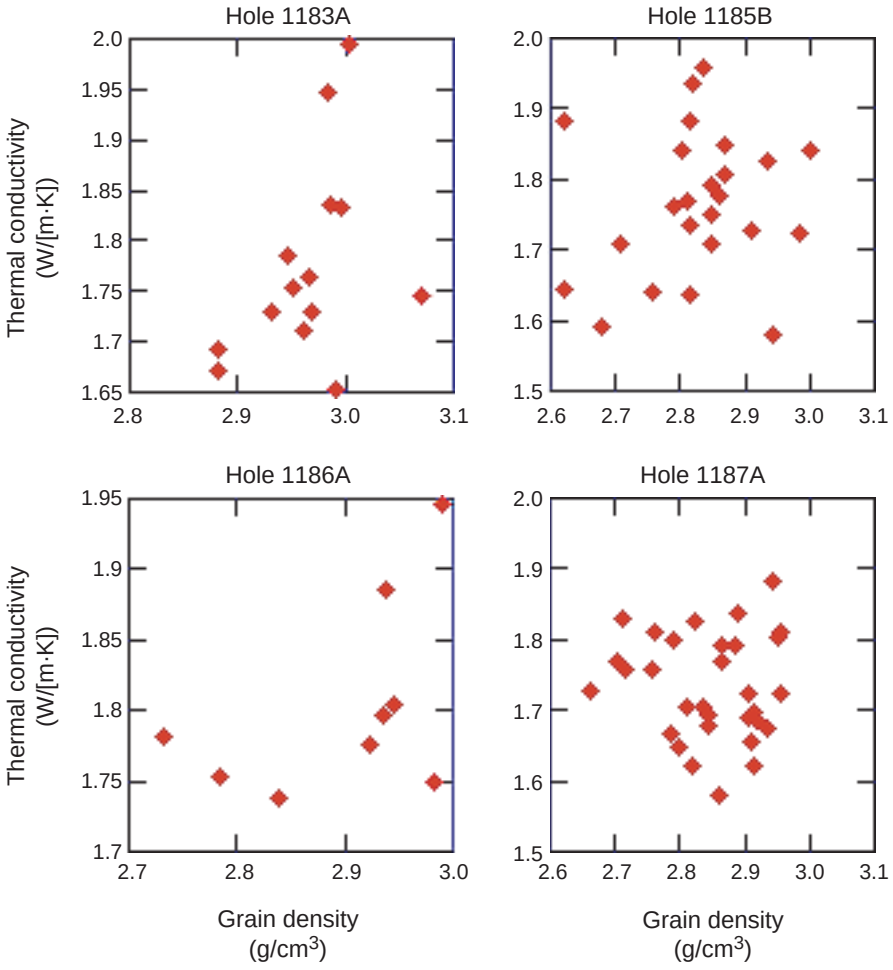

Table T1. Simplified hole summary of Leg 192 basement sites.

Hole	Location	Coordinates	Water depth (m)	Basement recovery (m)	Lithologic description	Number of units	Age (Ma)	Alteration (vol%)	LOI (wt%)	K_2O (wt%)	Veins/m
192-1183A	Crest of the main Ontong Java Plateau	1°10.6189′S 157°0.8988′E	1804.7	44.20	Submarine; basaltic lava flows	8	120–122	<5–20	0.6–2.4	0.07–0.58	19
1185A	Eastern edge of the main Ontong Java Plateau	0°21.4560′S 161°40.0619′E	3898.9	11.17	Submarine; pillow basalt	5	120–122		–0.19–0.79	0.08–0.28	28
1185B	Eastern edge of the main Ontong Java Plateau	0°21.4559′S 161°40.0511′E	3898.9	90.68	Submarine; pillow basalt	12	120–122		–0.58–2.54	0.03–1.00	25
1186A	Eastern slope of the main Ontong Java Plateau	0°40.7873′S 159°50.6519′E	2728.7	39.36	Submarine; pillow basalt	4	120–122	5–30	0.38–2.11	0.02–0.61	18
1187A	Eastern edge of the main Ontong Java Plateau	0°56.5518′N 161°27.0784′E	3803.6	100.87	Submarine; pillow lava flows	12	120–122	Greatest overall	0.86–3.48	0.03–0.97	~25

Notes: New basement ages reported by Chambers et al. (2002, 2004) and Parkinson et al. (2001). Alteration estimated visually by color distribution in hand specimen and confirmed by thin section study (Mahoney, Fitton, Wallace, et al., 2001). LOI = weight loss on ignition at 1100°C, K_2O = potassium (Mahoney, Fitton, Wallace, et al., 2001). A vein log for Hole 1187A was not compiled, but Banerjee et al. (2004) inferred that vein density for Hole 1187A would be similar to that in Hole 1185B.

Table T2. P-wave velocity, selected geochemical data, and vein logs for basalts at Sites 1183, 1185, 1186, and 1187. (**See table notes.** Continued on next six pages.)

Core, section, interval (cm)	Depth (mbsf)	Measurement type	Velocity (m/s)	LOI (wt%)	K_2O (wt%)	Vein measurements: length (cm)	Vein measurements: width (mm)	Basement unit
192-1183A-								
54R-5, 36–38	1132.49	Mx	5417.5			1	Hf	2B
55R-3, 131–133	1140.45	Mx	4768.3	1.75	0.07	2	<1	4B
56R-3, 18–20	1149.11	Mx	5232.5			5	<1	5B
57R-1, 131–133	1152.31	Mx	5553.1			1	Hf	5B
58R-3, 58–60	1159.19	Mx	5254.7	0.30	0.10	<1	H	5B
59R-1, 60–62	1161.20	Mx	5824.7			3	Hf	5B
59R-1, 60–62	1161.20	_x	5923.4	–0.59	BD			
59R-1, 113–115	1161.73	_x	5662.2					
59R-2, 65–67	1162.70	_x	5643.5					
60R-1, 136–138	1167.86	Mx	5253.1	0.09	0.09			
60R-1, 144–146	1167.94	_x	5736.9					
60R-2, 9–11	1168.07	_x	4728.6					
61R-1, 8–10	1176.18	_x	5604.6					
61R-1, 74–76	1176.84	_x	5603.9					
61R-1, 76–78	1176.86	_x	5064.7			0	Hf	5C
61R-1, 134–136	1177.44	Mx	5851.5					
61R-2, 7–9	1177.55	_x	5769.5					
61R-2, 52–54	1178.00	_x	4921.4			6	<1	5C
62R-1, 63–65	1181.63	Mx	5868.0			0	Hf	5C
62R-1, 70–72	1181.70	_x	5910.7					
62R-1, 115–117	1182.15	_x	5289.7					
62R-2, 100–102	1183.40	_x	5343.6					
62R-2, 145–147	1183.85	_x	5426.6			0	Hf	5C
62R-3, 35–37	1184.25	_x	5500.6			8	<1–1.5	5C
63R-1, 94–96	1186.74	Mx	5485.1					
63R-1, 115–117	1186.95	_x	5025.7			2	<1	5C
63R-1, 125–127	1187.05	_x	5648.2			5	Hf	5C
63R-2, 26–28	1187.46	_x	5112.5			4	<1	5C
64R-1, 85–87	1191.45	_x	5175.3			4	<1	5C
64R-2, 75–77	1192.75	_x	5942.0	0.57	0.10			
64R-2, 81–83	1192.81	Mx	5809.1			6	Hf	6B
64R-2, 130–132	1193.30	_x	5493.9	0.19	0.51	4	<1	6B
65R-1, 15–17	1195.55	_x	5596.8			4	<1–1.5	6B
65R-1, 40–42	1195.80	_x	5754.0					
65R-1, 45–47	1195.85	Mx	5531.8			2	<1	6B
65R-1, 90–92	1196.30	_x	5704.0					
65R-1, 120–122	1196.60	_x	5793.8					
65R-2, 39–41	1197.19	_x	5498.4					
65R-2, 120–122	1198.00	_x	5625.4			2	Hf	6B
65R-3, 26–28	1198.42	_x	5480.4	0.29	BD	6	Hf	6B
65R-3, 90–92	1199.06	_x	5487.1			2	Hf	6B
66R-1, 46–48	1200.56	_x	5679.4					
66R-1, 133–135	1201.43	_x	4626.8					
66R-2, 10–12	1201.60	_x	5728.4			11	<1	6B
66R-2, 86–88	1202.36	_x	5285.2					
66R-2, 140–142	1202.90	_x	5699.6					
66R-3, 10–12	1203.04	_x	5654.3					
66R-3, 12–14	1203.06	Mx	5845.1			0	<1	6B
66R-3, 54–56	1203.48	_x	5585.3			1	Hf	6B
67R-1, 2–4	1204.92	Mx	5488.8					
67R-1, 15–17	1205.05	_x	5265.0					
67R-1, 18–20	1205.08	_x	5841.4					
67R-1, 50–52	1205.40	_x	5478.9					
67R-1, 92–94	1205.82	_x	5763.0					
67R-1, 137–139	1206.27	_x	5438.9					
67R-2, 8–10	1206.43	_x	5747.7			1	Hf	6B
67R-2, 58–60	1206.93	_x	5696.4					
67R-2, 98–100	1207.33	_x	5324.5			3	Hf	6B
68R-1, 13–15	1209.83	_x	5850.0	0.19	0.14			
68R-1, 30–32	1210.00	_x	5487.1					
68R-1, 40–42	1210.10	Mx	5159.6			1	<1	6B

Table T2 (continued).

Core, section, interval (cm)	Depth (mbsf)	Measurement type	Velocity (m/s)	LOI (wt%)	K_2O (wt%)	Vein measurements: length (cm)	Vein measurements: width (mm)	Basement unit
192-1185A-								
8R-2, 89–91	310.80	_x	5506.2	–0.19	0.18	3	<1–2	
8R-2, 55–57	310.46	_x	5312.1					
9R-1, 54–56	317.55	_x	5140.8			0	Hf	
9R-2, 49–51	319.00	_x	5202.0	0.79	0.28			
9R-3, 69–71	320.68	_x	4796.4			3	<1	
9R-4, 79–81	322.28	_x	4641.4			2	Hf	
10R-1, 85–87	323.46	_x	4750.1			5	Hf	
10R-3, 38–40	325.66	Mx	5612.1	0.59	0.08			
10R-3, 59–61	325.87	_x	4802.0			7	Hf	
11R-1, 44–46	328.15	_x	5455.8					
192-1185B-								
3R-1, 79–81	316.50	_x	4189.1	–0.28	0.12	2	Hf	1
3R-2, 69–71	317.80	_x	4038.0			0	1	1
4R-1, 79–81	320.00	_x	4208.4			2	Hf	1
4R-2, 22–24	320.93	_x	5155.5			2.0	<1	2
4R-3, 49–51	321.67	_x	5263.5					
4R-4, 109–111	323.63	Mx	5193.2			1.0	<1	2
4R-4, 139–141	323.93	_x	5142.3			2.0	Hf	2
4R-5, 49–51	324.50	_x	5059.6			2.0	<1	2
4R-6, 29–31	325.51	_x	5169.9					
4R-7, 39–41	326.73	_x	5008.0	1.22	0.09	2.0	<1	2
5R-1, 25–27	329.06	Mx	5230.6					
5R-1, 34–36	329.15	_x	5306.5			6.0	1–2	2
5R-1, 99–101	329.80	_x	5513.6			2.5	Hf	2
5R-2, 59–61	330.47	_x	5382.8	0.69	0.07			
5R-3, 49–51	331.78	_x	5378.6					
5R-4, 21–23	332.58	_x	5410.8					
5R-4, 39–41	332.76	_x	5426.3					
5R-5, 109–111	334.73	_x	5407.8					
5R-6, 23–25	335.37	Mx	5334.8					
5R-6, 39–41	335.53	_x	5429.4					
5R-7, 105–107	337.64	_x	4369.3			11.0	<1–2	2
5R-7, 120–122	337.79	_x	4178.7			3.0	Hf	2
5R-7, 139–141	337.98	_x	4594.8			5.0	1–2	2
5R-8, 2–4	338.07	Mx	4713.4			1.5	1–3	2
5R-8, 7–9	338.12	_x	4419.7			5.5	<1–2	2
6R-2, 42–44	339.90	Mx	5691.0					
6R-2, 59–61	340.07	_x	5496.8			3.0	<1	5
6R-3, 89–91	341.43	_x	5065.3			0.0	<1	5
6R-4, 29–31	342.22	_x	5485.2	1.31	0.03			
6R-5, 107–109	344.43	_x	5476.6					
6R-5, 132–134	344.68	Mx	5477.3					
6R-6, 72–74	345.53	_x	5647.3					
7R-1, 94–96	349.05	_x	4663.5			6.0	1–2	6
7R-2, 79–81	350.40	_x	4327.9			4.0	15	7
7R-3, 16–18	351.27	Mx	4485.9			4.0	Hf	7
7R-3, 17–19	351.28	_x	4498.8					
7R-4, 4–6	352.54	_x	4658.4			5.0	Hf	7
8R-1, 35–37	358.06	_x	4859.1			11.0	<1–1.5	7
8R-1, 94–96	358.65	_x	4703.1			5.0	2	7
8R-1, 96–98	358.67	Mx	4999.3			2.0	Hf	7
8R-2, 4–6	359.25	_x	5126.4	2.54	0.23	1.0	Hf	7
9R-1, 42–44	367.73	_x	4856.7			1.0	1–2	7
9R-2, 114–116	369.82	_x	4735.5			2	Hf	9
9R-3, 34–36	370.51	_x	5066.7			1.5	<1–4	9
10R-1, 87–89	377.78	_x	4788.9			4.0	<1–2	9
10R-2, 26–28	378.63	Cx	4720.8			6.0	<1	9
10R-2, 26–28	378.63	Cz	5110.6					
10R-2, 54–56	378.91	_x	5050.2			0.5	<1	9
11R-1, 14–16	386.65	_x	5309.5					
11R-1, 114–116	387.65	_x	4996.0	2.46	0.71	5.0	<1	9
12R-1, 39–41	396.50	_x	4815.6			13.0	<1–1	9
13R-1, 19–21	400.40	_x	4132.5					
14R-2, 23–25	407.44	_x	4241.4			17.0	1–2	9
14R-2, 109–111	408.30	_x	4555.2			5.0	2	9
14R-3, 24–26	408.95	_x	4340.3	2.26	0.16	6.0	1	9

Table T2 (continued).

Core, section, interval (cm)	Depth (mbsf)	Measurement type	Velocity (m/s)	LOI (wt%)	K_2O (wt%)	Vein measurements		Basement unit
						length (cm)	width (mm)	
15R-1, 77–79	416.08	_x	4336.9					
15R-2, 4–6	416.85	_x	4318.2			3.0	<1–1	9
15R-2, 90–92	417.71	_x	4958.7					
15R-3, 49–51	418.71	_x	4675.2			4.5	<1	9
16R-1, 34–36	425.25	_x	5175.9			1.0	1–2	9
16R-1, 39–41	425.30	Mx	4968.7					
16R-1, 45–47	425.36	_x	5184.2					
17R-1, 47–49	435.08	_x	5322.2			1.0	<1	10
17R-2, 39–41	436.10	_x	5583.6			1.0	<1	10
17R-2, 84–86	436.55	Mx	4879.4			6.0	1	10
17R-3, 9–11	437.21	_x	5465.2	0.59	0.08			
17R-3, 69–71	437.81	_x	5122.6					
17R-4, 13–15	438.68	_x	5190.6			3.0	<1–1	10
18R-1, 17–19	444.48	_x	5364.6					
18R-1, 97–99	445.28	_x	4636.5					
18R-2, 23–25	446.04	_x	5598.6	0.48	0.07			
19R-1, 32–34	449.43	_x	5689.5					
19R-2, 34–36	450.90	_x	5667.0			1.0	<1	10
19R-2, 111–113	451.67	Mx	5541.3					
19R-3, 29–31	452.30	_x	5243.5					
19R-3, 78–81	452.77	Mx	5699.9			1.0	1	10
19R-4, 74–76	453.79	_x	5198.0					
20R-1, 109–111	455.00	_x	4693.4					
20R-2, 22–24	455.38	Mx	5601.8					
20R-2, 119–121	456.35	_x	5332.7			3.0	Hf	11
20R-3, 63–65	457.07	_x	5295.9	0.19	0.06			
20R-4, 81–83	458.11	_x	5570.5			1.0	<1	11
21R-1, 79–81	464.40	_x	5425.0			2.0	<1	11
21R-1, 109–111	464.70	_x	5685.7					
21R-2, 59–61	465.39	_x	5253.1			4.0	<1	11
21R-2, 99–101	465.79	_x	5607.7					
21R-3, 37–39	466.23	_x	5712.1					
21R-3, 38–40	466.24	_x	5541.8					
21R-3, 99–101	466.85	_x	5725.6			2.0	<1	11
21R-4, 56–58	467.74	_x	5680.8					
21R-4, 89–91	468.07	_x	5619.6					
21R-5, 9–11	468.53	_x	5716.9					
21R-5, 108–110	469.52	Mx	5449.4					
21R-5, 109–111	469.53	_x	5661.7					
21R-6, 39–41	470.17	_x	5542.4					
21R-6, 139–141	471.17	_x	5487.9					
21R-7, 35–37	471.58	Mx	5790.1					
21R-7, 36–38	471.59	_x	5681.6					
21R-8, 89–91	473.54	_x	5259.3			1	Hf	11
21R-8, 119–121	473.84	_x	5307.9					
22R-2, 79–81	475.36	_x	5162.1					
22R-2, 82–84	475.39	Mx	5472.8					
22R-3, 14–16	476.11	_x	5174.9					
22R-4, 49–51	477.83	_x	5610.2					
22R-5, 91–93	479.75	_x	5141.5					
22R-6, 88–90	481.19	_x	5071.9	0.79	0.07			
22R-7, 3–5	481.68	_x	5177.8	0.59	1.00			
23R-1, 59–61	483.40	_x	5151.0					
23R-2, 81–83	485.12	_x	4681.7					
23R-2, 89–91	485.20	Mx	5102.6					
24R-1, 33–35	492.84	_x	4873.3			1.0	<1–1.5	12
24R-2, 78–80	494.78	Cx	5314.5					
24R-2, 78–80	494.78	Cy	5527.9					
24R-2, 78–80	494.78	Cz	5271.6					
24R-2, 109–111	495.09	_x	4767.5			12.0	<1	12
28R-1, 17–19	517.78	Mx	5598.7					
28R-1, 77–79	518.38	_x	5420.1	0.48	0.08			
192-1186A-								
30R-1, 59–61	967.00	_x	5023.9	1.43	0.61			
30R-2, 9–11	967.86	_x	5371.7			2	Hf	1
30R-2, 16–18	967.93	Cx	5436.1					
30R-2, 16–18	967.93	Cy	5521.3					

Table T2 (continued).

Core, section, interval (cm)	Depth (mbsf)	Measurement type	Velocity (m/s)	LOI (wt%)	K_2O (wt%)	Vein measurements		Basement unit
						length (cm)	width (mm)	
30R-2, 16–18	967.93	Cz	5536.2					
30R-2, 25–27	968.02	_x	4831.1			5	Hf	1
30R-2, 37–39	968.14	_x	5531.2					
30R-2, 69–71	968.46	_x	5354.0			0.5	Hf	1
31R-1, 19–21	970.20	_x	4661.2	1.39	0.02	7.0	<1	1
31R-1, 67–69	970.68	_x	5505.1			2.5	<1	1
31R-2, 22–24	971.72	_x	4963.1			3	Hf	1
31R-3, 5–7	972.82	_x	5525.1					
31R-3, 59–61	973.36	_x	5118.6					
31R-4, 51–53	974.38	_x	5005.1	2.11	0.05			
32R-1, 66–68	976.87	_x	5446.1					
32R-2, 9–11	977.77	_x	5144.0					
32R-3, 49–51	979.67	_x	4969.3			3.0	<1	1
32R-4, 49–51	981.16	_x	5286.7					
33R-1, 63–65	981.64	_x	5699.6	0.38	0.09			
33R-2, 39–41	982.45	_x	5575.6					
33R-2, 109–111	983.15	_x	5476.7					
33R-3, 29–31	983.55	_x	5694.5					
34R-1, 9–11	985.90	_x	5685.0					
34R-1, 19–21	986.00	_x	5324.9					
34R-1, 89–91	986.70	_x	5457.5					
34R-1, 137–139	987.18	_x	5663.4					
34R-2, 9–11	987.33	_x	5522.1					
34R-2, 24–26	987.48	Mx	5812.9					
34R-2, 35–37	987.59	_x	5718.0					
34R-2, 74–76	987.98	_x	5714.0					
34R-2, 142–144	988.66	_x	5490.9			2.0	<1	2B
34R-3, 54–56	989.24	_x	5689.5					
34R-4, 55–57	990.75	_x	4611.7	0.58	0.40			
34R-5, 97–99	992.67	_x	5192.3			0	Hf	3B
34R-6, 4–6	993.22	_x	4993.0					
34R-6, 23–25	993.41	_x	5035.9			2.0	<1	3B
34R-6, 102–104	994.20	_x	5418.7			1.5	Hf	3B
35R-1, 71–73	996.22	_x	4638.6			3.0	<1	3B
35R-1, 111–113	996.62	_x	5164.9					
35R-2, 32–34	997.32	_x	5002.5					
35R-2, 84–86	997.84	_x	4429.4					
37R-1, 46–48	1015.27	_x	5130.8	1.10	0.12			
37R-1, 115–117	1015.96	_x	4661.2			2	Hf	3B
37R-2, 31–33	1016.57	_x	5153.7					
37R-3, 29–31	1017.13	_x	5788.9					
37R-3, 111–113	1017.95	_x	5231.8					
38R-1, 4–6	1019.45	_x	5989.0					
38R-1, 19–21	1019.60	_x	5658.5					
38R-1, 69–71	1020.10	_x	5497.0					
38R-1, 99–101	1020.40	_x	5083.0					
38R-1, 139–141	1020.80	Mx	5345.3					
38R-2, 7–9	1020.93	_x	4793.5					
38R-2, 49–51	1021.35	_x	5355.7			0	Hf	3B
38R-2, 137–139	1022.23	_x	5075.7					
38R-3, 9–11	1022.40	_x	5470.5					
38R-3, 65–67	1022.96	Cx	5395.1					
38R-3, 65–67	1022.96	Cy	5347.1					
38R-3, 65–67	1022.96	Cz	5270.3					
38R-3, 96–98	1023.27	_x	5127.0					
38R-4, 7–9	1023.80	_x	5454.8					
39R-1, 4–6	1024.45	_x	5435.2					
38R-4, 99–101	1024.72	_x	5538.9					
38R-4, 130–132	1025.03	Mx	5481.3					
39R-1, 100–102	1025.41	Cx	5452.9			2	Hf	3B
39R-1, 100–102	1025.41	Cy	5403.1					
39R-1, 100–102	1025.41	Cz	5483.7					
39R-2, 1–3	1025.74	Mx	5417.0			2.0	<1	3B
39R-2, 104–106	1026.77	_x	5360.6					
39R-3, 49–51	1027.39	_x	5519.7					
39R-3, 93–95	1027.83	Cx	5558.1					
39R-3, 93–95	1027.83	Cy	5554.8					

Table T2 (continued).

Core, section, interval (cm)	Depth (mbsf)	Measurement type	Velocity (m/s)	LOI (wt%)	K_2O (wt%)	Vein measurements		Basement unit
						length (cm)	width (mm)	
39R-3, 93–95	1027.83	Cz	5711.3					
39R-4, 9–11	1028.45	_x	5229.0					
39R-4, 50–52	1028.86	Mx	5908.0					
39R-5, 9–11	1029.51	_x	5546.0	1.00	0.05			
39R-5, 29–31	1029.71	_x	5464.4					
39R-5, 47–49	1029.89	_x	5460.0			1.0	<1	3B
39R-5, 69–71	1030.11	_x	5584.6					
39R-5, 99–101	1030.41	_x	5262.1			0.0	<1	3B
192-1187A-								
2R-2, 84–86	367.53	_x	4820.3					
2R-2, 85–87	367.54	Mx	5039.6					
2R-2, 97–99	367.66	_x	4852.9					
2R-2, 117–119	367.86	_x	4956.9					
3R-1, 6–8	374.57	_x	4585.3					
3R-1, 83–85	375.34	_x	4959.9					
3R-2, 34–36	376.31	_x	5091.1					
3R-2, 53–55	376.50	Mx	4741.4					
3R-2, 54–56	376.51	_x	4957.9					
3R-2, 104–106	377.01	_x	4945.4					
3R-2, 129–131	377.26	_x	4697.5					
3R-3, 11–13	377.56	_x	4736.6					
3R-3, 63–65	378.08	Mx	5043.0					
3R-3, 64–66	378.09	_x	5041.0	1.79	0.22			
3R-3, 117–119	378.62	_x	4753.5					
3R-4, 12–14	379.02	_x	5143.4					
3R-4, 119–121	380.09	_x	4798.2					
3R-5, 34–36	380.73	_x	4813.5					
3R-5, 64–66	381.03	_x	5056.4					
3R-5, 104–106	381.43	_x	5129.4					
4R-1, 25–27	384.46	Mx	5396.8					
4R-1, 36–38	384.57	_x	4918.9					
4R-1, 99–101	385.20	_x	4841.1					
4R-2, 39–41	386.09	_x	4925.5					
4R-2, 129–131	386.99	_x	4686.3	2.46	0.32			
4R-3, 95–97	388.15	_x	4561.1					
4R-4, 43–45	389.13	_x	4936.8					
4R-4, 103–105	389.73	_x	5060.7					
4R-5, 26–28	390.13	_x	4662.1					
4R-5, 87–89	390.74	_x	5081.3					
4R-6, 29–31	391.66	_x	5000.9					
5R-1, 24–26	394.05	_x	5293.2					
5R-1, 24–26	394.05	Mx	4894.8					
5R-1, 114–116	394.95	_x	4973.4					
5R-2, 32–34	395.51	_x	4948.8					
5R-2, 109–111	396.28	_x	5296.0					
5R-3, 58–60	397.27	_x	4780.9					
5R-3, 90–92	397.59	Mx	4931.4					
5R-3, 109–111	397.78	_x	5526.7					
5R-4, 59–61	398.71	_x	5530.6					
5R-4, 121–123	399.33	Mx	5175.8					
5R-4, 134–136	399.46	_x	5305.9					
5R-5, 52–54	400.14	_x	4932.7					
5R-5, 99–101	400.61	_x	5407.4					
5R-6, 114–116	402.26	_x	5126.0					
5R-7, 15–17	402.56	_x	5013.6					
5R-8, 35–37	403.95	_x	5370.0					
6R-1, 34–36	403.75	_x	5006.0					
6R-1, 101–103	404.42	_x	4959.9					
6R-2, 119–121	405.83	_x	5163.4					
6R-3, 44–46	406.58	_x	4911.0					
6R-3, 99–101	407.13	_x	5106.6					
6R-4, 19–21	407.78	_x	5015.7					
6R-4, 49–51	408.08	_x	4541.2					
6R-5, 29–31	408.47	_x	5228.0					
6R-5, 69–71	408.87	_x	4972.7					
6R-6, 64–66	410.18	_x	5173.5					
6R-6, 86–88	410.40	_x	5150.0					
6R-6, 89–91	410.43	_x	5488.7	0.86	0.04			

Table T2 (continued).

Core, section, interval (cm)	Depth (mbsf)	Measurement type	Velocity (m/s)	LOI (wt%)	K_2O (wt%)	Vein measurements		Basement unit
						length (cm)	width (mm)	
6R-6, 124–126	410.78	_x	5483.8					
6R-7, 4–6	410.89	_x	5485.8					
6R-7, 51–53	411.36	_x	5304.8					
6R-7, 109–111	411.94	_x	5146.7					
7R-1, 34–36	413.35	_x	5434.8					
7R-1, 139–141	414.40	_x	4647.3					
7R-2, 29–31	414.77	_x	4694.8					
7R-2, 79–81	415.27	_x	4723.7					
7R-3, 15–17	415.89	_x	4714.0					
7R-3, 74–76	416.48	_x	5708.6					
7R-4, 31–33	417.24	Mx	5278.2					
7R-4, 79–81	417.72	_x	4732.5					
7R-5, 24–26	418.47	_x	4781.4					
7R-5, 89–91	419.12	_x	4950.5					
7R-6, 37–39	419.68	_x	5082.2	3.48	0.97			
7R-7, 22–24	420.56	_x	5006.5					
7R-7, 97–99	421.31	Mx	5831.4					
8R-1, 65–67	423.26	_x	4836.0					
8R-2, 19–21	424.19	_x	4561.5					
8R-2, 99–101	424.99	_x	4709.6					
8R-3, 42–44	425.77	_x	4772.6					
8R-3, 59–61	425.94	Mx	5180.8					
8R-4, 55–57	427.39	_x	5059.4					
8R-4, 105–107	427.89	_x	5231.8					
8R-5, 39–41	428.54	_x	4973.1					
8R-5, 107–109	429.22	_x	5536.1					
8R-6, 16–18	429.67	_x	5768.1					
8R-6, 72–74	430.23	Mx	5392.5					
8R-6, 89–91	430.40	_x	5585.1					
8R-7, 34–36	431.22	_x	5464.7					
9R-1, 44–46	432.75	_x	5052.0					
9R-1, 89–91	433.20	_x	4550.9					
9R-2, 13–15	433.82	_x	5131.5					
9R-3, 14–16	435.24	_x	5416.3					
9R-3, 69–71	435.79	_x	5826.0					
9R-4, 24–26	436.35	_x	5542.5	1.03	0.11			
9R-4, 109–111	437.20	_x	5450.1					
9R-5, 5–7	437.57	Mx	5175.9					
9R-5, 59–61	438.11	_x	5224.5					
9R-5, 87–89	438.39	_x	5537.9					
9R-6, 64–66	439.62	_x	5050.4					
9R-6, 119–121	440.17	_x	4617.3					
9R-7, 33–35	440.77	_x	4831.9					
10R-1, 11–13	442.02	Mx	5271.2					
10R-1, 44–46	442.35	_x	4637.0					
10R-1, 69–71	442.60	_x	4435.9					
10R-2, 47–49	443.88	_x	4690.6					
10R-2, 106–108	444.47	_x	4987.1					
10R-3, 49–51	445.40	_x	5432.8					
10R-3, 97–99	445.88	_x	5172.8					
10R-4, 49–51	446.62	_x	4839.4					
10R-4, 122–124	447.35	_x	5521.5					
10R-5, 17–19	447.59	_x	5563.0					
10R-5, 39–41	447.81	Mx	5870.1					
10R-6, 47–49	448.80	_x	4997.0					
10R-6, 92–94	449.25	_x	5759.2					
10R-7, 6–8	449.66	_x	5681.9	1.20	0.03			
10R-7, 86–88	450.46	_x	4718.1					
11R-1, 17–19	451.68	_x	5002.3					
11R-1, 107–109	452.58	_x	4907.8					
11R-2, 22–24	452.93	_x	5285.0					
11R-2, 113–115	453.84	_x	4904.7					
11R-3, 1–3	454.22	Mx	4561.7					
11R-3, 94–96	455.15	_x	4938.8					
11R-4, 32–34	455.53	_x	5330.8					
11R-4, 134–136	456.55	_x	4913.7					
11R-5, 30–32	456.91	Mx	5439.1					

Table T2 (continued).

Core, section, interval (cm)	Depth (mbsf)	Measurement type	Velocity (m/s)	LOI (wt%)	K_2O (wt%)	Vein measurements		Basement unit
						length (cm)	width (mm)	
11R-5, 119–121	457.80	_x	5223.2					
11R-6, 34–36	458.39	_x	4826.7					
12R-1, 7–9	461.18	_x	5132.2					
12R-1, 131–133	462.42	_x	4687.0					
12R-2, 45–47	463.04	_x	4870.5					
12R-2, 109–111	463.68	_x	5324.0					
12R-3, 99–101	465.04	_x	5133.7					
12R-4, 3–5	465.43	_x	5106.4					
12R-4, 103–105	466.43	_x	4962.4					
12R-5, 41–43	466.97	_x	5393.8					
12R-5, 79–81	467.35	Mx	5292.6	0.98	0.07			
12R-5, 97–99	467.53	_x	4790.4					
13R-1, 43–45	471.14	_x	4776.9					
13R-1, 104–106	471.75	_x	5594.3					
13R-2, 29–31	472.29	_x	5415.2					
13R-2, 31–33	472.31	Mx	5779.6					
13R-2, 107–109	473.07	_x	5295.0					
13R-3, 89–91	474.28	_x	5743.4					
13R-4, 14–16	474.82	_x	5468.9					
13R-4, 95–97	475.63	_x	5416.1					
13R-5, 49–51	476.17	_x	5447.6					
13R-5, 61–63	476.29	Mx	5323.1					
13R-5, 129–131	476.97	_x	5224.2					
13R-6, 23–25	477.41	_x	4840.2					
14R-1, 64–66	480.95	_x	4871.1					
14R-1, 119–121	481.50	_x	4690.1					
14R-2, 35–37	482.16	Mx	4949.0					
14R-2, 39–41	482.20	_x	4644.0					
14R-3, 27–29	483.46	Mx	5175.2					
14R-3, 33–35	483.52	_x	4677.6					
14R-3, 138–140	484.57	_x	4716.5					
14R-4, 7–8	484.76	_x	5028.3					
15R-2, 39–41	491.25	_x	5423.4					
15R-2, 75–77	491.61	_x	4751.6					
15R-3, 41–43	492.54	_x	5139.8					
15R-3, 87–89	493.00	Mx	5300.2					
15R-3, 104–106	493.17	_x	5828.7					
15R-4, 9–10	493.57	_x	5308.4					
15R-4, 19–21	493.67	Mx	5298.0					
15R-4, 59–61	494.07	_x	5302.8					
16R-1, 7–8	499.78	_x	5030.9					
16R-1, 69–71	500.40	_x	4931.9					
16R-2, 19–21	500.84	_x	4588.6					
16R-2, 113–115	501.78	_x	4799.1					
16R-3, 44–46	502.48	_x	5090.6					
16R-3, 115–117	503.19	_x	4566.6					
16R-4, 15–17	503.52	_x	4559.9					
16R-4, 105–107	504.42	_x	4268.8					
16R-5, 27–29	505.10	_x	4687.1					
16R-5, 89–91	505.72	_x	4705.9					

Notes: _ = uncut split core, C = cut sample, M = minicore. x = into the core, y = across the core, z = along the core. All geochemical data after Mahoney, Fitton, Wallace, et al. (2001). LOI = weight loss on ignition, K_2O = potassium content. BD = below detection. Vein logs after **Banerjee and Honnorez** (this volume). Hf = hairline fracture. Vein log for Site 1187 was not compiled.

Table T3. Summary of moisture and density (MAD) for basalts at Sites 1183, 1185, 1186, and 1187.

Core, section, interval (cm)	Depth (mbsf)	Density (g/cm3)			Porosity (%)
		Bulk	Dry	Grain	
192-1183A-					
54R-1, 88–90	1127.68	2.444	2.264	2.748	17.622
54R-5, 36–38	1132.49	2.727	2.641	2.883	8.410
55R-3, 131–133	1140.45	2.611	2.462	2.881	14.527
56R-3, 18–20	1149.11	2.749	2.634	2.968	11.240
57R-1, 131–133	1152.31	2.794	2.684	3.004	10.648
58R-3, 58–60	1159.19	2.689	2.545	2.962	14.076
59R-1, 60–62	1161.20	2.892	2.844	2.984	4.700
60R-1, 136–138	1167.86	2.703	2.564	2.966	13.562
61R-1, 134–136	1177.44	2.858	2.811	2.947	4.613
62R-1, 63–65	1181.63	2.932	2.899	2.996	3.240
63R-1, 94–96	1186.74	2.845	2.769	2.991	7.406
65R-1, 45–47	1195.85	2.670	2.506	2.986	16.092
66R-3, 12–14	1203.06	2.695	2.560	2.950	13.226
67R-1, 2–4	1204.92	2.749	2.650	2.932	9.604
68R-1, 40–42	1210.10	2.934	2.866	3.070	6.631
192-1185A-					
2R-1, 77–79	251.38	1.537	0.941	2.250	58.183
2R-2, 59–61	252.70	1.557	0.968	2.279	57.538
3R-1, 62–64	260.83	1.647	1.033	2.580	59.960
3R-2, 19–21	261.90	1.688	1.096	2.598	57.827
4R-1, 25–27	270.06	1.509	0.879	2.284	61.507
5R-1, 24–26	279.75	1.548	0.953	2.274	58.076
6R-1, 8–10	289.19	1.543	0.936	2.298	59.293
7R-1, 132–134	300.13	1.469	0.865	2.108	58.953
7R-2, 2–4	300.33	1.497	0.908	2.137	57.532
10R-3, 39–41	325.67	2.557	2.437	2.762	11.772
192-1185B-					
2R-1, 43–45	308.43	1.867	1.384	2.618	47.118
4R-4, 111–113	323.64	2.708	2.630	2.846	7.586
5R-1, 26–28	329.06	2.649	2.537	2.849	10.941
5R-6, 24–26	335.37	2.666	2.581	2.816	8.363
5R-8, 3–5	338.07	2.536	2.375	2.818	15.727
6R-2, 43–45	339.90	2.644	2.536	2.836	10.574
6R-5, 133–135	344.68	2.729	2.614	2.944	11.236
7R-3, 16–18	351.26	2.438	2.320	2.621	11.466
8R-1, 96–98	358.66	2.543	2.443	2.708	9.764
10R-2, 27–29	378.63	2.595	2.469	2.815	12.281
12R-1, 66–68	396.76	2.484	2.395	2.622	8.640
14R-3, 54–56	409.24	2.576	2.450	2.792	12.239
15R-2, 62–63	417.42	2.561	2.488	2.679	7.149
16R-1, 40–42	425.30	2.519	2.379	2.757	13.715
17R-2, 84–86	436.54	2.854	2.811	2.935	4.210
18R-1, 12–14	444.42	2.747	2.682	2.862	6.266
19R-1, 37–39	449.47	2.725	2.625	2.908	9.753
19R-2, 112–114	451.67	2.748	2.682	2.867	6.457
20R-2, 23–25	455.38	2.707	2.627	2.849	7.823
21R-5, 109–111	469.52	2.789	2.744	2.870	4.404
21R-7, 36–38	471.58	2.736	2.698	2.801	3.679
22R-2, 83–85	475.39	2.698	2.631	2.815	6.518
23R-2, 89–91	485.19	2.729	2.682	2.811	4.589
24R-2, 79–81	494.78	2.803	2.708	2.985	9.272
28R-1, 18–20	517.78	2.830	2.742	3.001	8.641
192-1186A-					
30R-2, 17–19	967.93	2.829	2.749	2.983	7.853
31R-1, 11–13	970.11	2.544	2.431	2.731	10.972
31R-3, 6–8	972.82	2.733	2.635	2.912	9.508
32R-1, 141–143	977.61	2.666	2.572	2.831	9.129
32R-3, 39–41	979.56	2.609	2.479	2.840	12.714
33R-1, 75–77	981.75	2.846	2.804	2.923	4.048
34R-2, 25–27	987.48	2.743	2.634	2.949	10.689
34R-4, 42–44	990.61	2.449	2.305	2.683	14.078
34R-6, 18–20	993.35	2.431	2.293	2.651	13.519
35R-1, 56–58	996.06	2.597	2.487	2.784	10.664
37R-1, 116–117	1015.96	2.575	2.464	2.763	10.834
37R-3, 28–30	1017.11	2.870	2.829	2.946	3.976
38R-1, 140–142	1020.80	2.809	2.739	2.939	6.806
38R-3, 66–68	1022.96	2.754	2.674	2.899	7.776
38R-4, 131–133	1025.03	2.704	2.617	2.860	8.476
39R-1, 101–103	1025.41	2.834	2.752	2.991	7.982
39R-2, 2–4	1025.74	2.594	2.466	2.820	12.547
39R-3, 94–96	1027.83	2.704	2.584	2.926	11.696
39R-4, 51–53	1028.86	2.782	2.700	2.935	7.993
192-1187A-					
2R-2, 86–88	367.54	2.630	2.476	2.914	15.047
3R-2, 54–56	376.50	2.565	2.412	2.836	14.968
3R-3, 64–66	378.08	2.657	2.551	2.845	10.359
4R-1, 25–27	384.45	2.761	2.680	2.911	7.922
4R-5, 65–67	390.51	2.552	2.454	2.714	9.559
5R-1, 23–25	394.03	2.624	2.547	2.756	7.580
5R-3, 90–92	397.58	2.640	2.568	2.763	7.057
5R-4, 121–123	399.32	2.869	2.823	2.957	4.527
6R-2, 108–110	405.71	2.667	2.579	2.820	8.559
6R-6, 56–58	410.09	2.672	2.587	2.822	8.325
7R-4, 32–34	417.24	2.626	2.525	2.800	9.825
7R-7, 98–100	421.31	2.653	2.516	2.905	13.400
8R-2, 64–66	424.63	2.569	2.444	2.785	12.242
8R-3, 59–61	425.93	2.802	2.738	2.920	6.231
8R-6, 72–74	430.22	2.590	2.518	2.710	7.083
9R-3, 91–93	436.00	2.764	2.668	2.944	9.361
9R-5, 6–8	437.57	2.582	2.450	2.812	12.878
10R-1, 12–14	442.02	2.493	2.388	2.662	10.264
10R-5, 40–42	447.81	2.708	2.621	2.863	8.428
11R-3, 2–4	454.22	2.472	2.331	2.702	13.736
11R-5, 31–33	456.91	2.759	2.658	2.950	9.880
12R-3, 46–48	464.50	2.685	2.617	2.804	6.655
12R-5, 79–81	467.34	2.738	2.655	2.889	8.079
13R-2, 31–33	472.30	2.771	2.735	2.835	3.535
13R-5, 61–63	476.28	2.771	2.709	2.885	6.111
14R-2, 36–38	482.16	2.630	2.502	2.859	12.494
14R-3, 28–30	483.46	2.699	2.580	2.917	11.559
14R-3, 146–148*	484.64	2.727		2.933	7.010
14R-4, 56–58*	485.24	2.689		2.863	6.060
15R-2, 75–77*	491.60	2.760		2.904	4.950
15R-3, 88–90	493.00	2.563	2.424	2.807	13.639
15R-3, 103–105*	493.15	2.725		2.956	7.820
15R-4, 20–22	493.67	2.584	2.465	2.789	11.637
16R-2, 37–39*	501.01	2.618		2.845	7.980
16R-3, 26–28*	502.28	2.800		2.912	3.860

Note: * = sample measured in the petrophysical laboratory at the First University of Naples, Italy.

Table T4. Magnetic susceptibility for basaltic pieces at Sites 1183, 1185, 1186, and 1187. (Continued on next two pages.)

Core, section, piece	Depth (mbsf)	Magnetic susceptibility (10^{-3} SI)
192-1183A-		
54R-5 (Piece 4)	1132.67	9.70
55R-1 (Piece 4)	1137.00	11.80
55R-2 (Piece 1)	1147.53	11.40
55R-3 (Piece 3)	1151.83	12.60
56R-1 (Piece 5)	1157.52	13.40
56R-1 (Piece 12)	1161.16	12.00
56R-2 (Piece 1)	1162.69	9.40
56R-2 (Piece 2)	1167.94	11.70
56R-2 (Piece 5)	1168.10	15.20
56R-2 (Piece 7)	1176.90	10.60
56R-3 (Piece 1)	1177.60	8.50
57R-3 (Piece 9)	1181.60	15.10
58R-3 (Piece 3)	1184.20	12.40
59R-1 (Piece 2)	1186.20	11.30
61R-1 (Piece 2)	1192.80	12.40
62R-2 (Piece 8)	1196.30	13.50
65R-1 (Piece 3)	1197.50	12.60
65R-2 (Piece 7)	1198.40	10.20
65R-3 (Piece 2)	1201.10	14.10
66R-1 (Piece 5)	1202.40	15.20
66R-1 (Piece 9)	1203.50	12.10
66R-3 (Piece 4)	1205.10	10.80
67R-1 (Piece 2)	1209.00	11.80
67R-1 (Piece 5)	1210.00	10.60
67R-2 (Piece 7)		14.80
192-1185A-		
8R-1(Piece 7)	309.06	4.46
8R2 (Piece 3)	310.24	8.30
8R-2 (Piece 4)	310.52	11.71
8R-2 (Piece 4)	310.79	10.18
8R-2 (Piece 4)	310.93	9.78
9R- (Piece 1)	317.15	18.85
9R-1 (Piece 6)	317.89	7.90
9R-1 (Piece 7)	318.03	8.84
9R-2 (Piece 1)	318.56	4.15
9R-2 (Piece 2)	318.77	7.61
9R-2 (Piece 3)	319.03	8.35
9R-2 (Piece 3)	319.23	7.37
9R-2 (Piece 6)	319.59	3.08
9R-3 (Piece 5)	320.58	7.44
9R-3 (Piece 8)	321.25	
10R-1 (Piece 8)	323.20	3.50
10R-1 (Piece 9)	323.42	9.13
10R-1 (Piece 9)	323.65	8.85
10R-2 (Piece1)	324.09	5.31
10R-2 (Piece 2)	324.32	5.86
11R-1 (Piece 4)	328.22	22.34
11R-1 (Piece 4)	328.46	24.77
192-1185B-		
3R-2 (Piece 1)	317.22	5.80
3R-2 (Piece 5)	317.50	4.20
3R-2 (Piece 7)	317.82	4.30
4R-3 (Piece 1)	321.26	7.70
4R-3 (Piece 1)	321.48	8.70
4R-3 (Piece 1)	321.81	9.00
4R-3 (Piece 1)	322.14	7.40
4R-3 (Piece 2)	322.42	6.90
4R-4 (Piece 1)	322.73	9.30
4R-4 (Piece 2)	323.21	9.60
4R-4 (Piece 2)	323.81	15.30
4R-5 (Piece 1)	324.13	7.50
4R-5 (Piece 2)	324.34	6.30
4R-5 (Piece 9)	325.14	7.70
4R-6 (Piece 1)	325.35	10.30
4R-6 (Piece 1)	325.66	13.20
4R-6 (Piece 1)	325.95	14.10
4R-6 (Piece 1)	326.19	14.90
4R-7 (Piece 1)	326.48	15.60
5R-1 (Piece 2)	329.06	16.40
5R-1 (Piece 2)	329.30	18.00
5R-1 (Piece 2)	329.72	13.70
5R-2 (Piece 1)	330.04	13.80
5R-2 (Piece 1)	330.21	12.70
5R-2 (Piece 1)	330.47	18.90
5R-2 (Piece 1)	330.80	23.50
5R-2 (Piece 1)	331.05	16.50
5R-3 (Piece 1)	331.42	13.50
5R-3 (Piece 1)	331.82	23.00
5R-3 (Piece 2)	332.13	16.90
5R-4 (Piece 1)	332.55	13.90
5R-4 (Piece 1)	332.79	17.10
5R-4 (Piece 1)	333.13	18.30
5R-4 (Piece 1)	333.25	12.90
5R-5 (Piece 1)	333.84	14.40
5R-5 (Piece 2)	334.31	27.70
5R-5 (Piece 2)	334.52	19.30
5R-5 (Piece 2)	334.88	28.50
5R-6 (Piece 1)	335.45	24.00
5R-6 (Piece 1)	335.77	14.70
5R-6 (Piece 1)	336.09	24.80
5R-7 (Piece 4)	337.09	7.00
5R-7 (Piece 7)	337.46	8.00
5R-7 (Piece 8)	337.65	8.00
5R-7 (Piece 11)	337.98	
6R-2 (Piece 1)	339.64	19.00
6R-2 (Piece 1)	339.95	29.30
6R-3 (Piece 4)	341.67	34.30
6R-4 (Piece 1)	342.05	27.90
6R-5 (Piece 1)	343.51	28.50
6R-5 (Piece 1)	343.71	28.20
6R-5 (Piece 1)	343.95	29.30
6R-5 (Piece 1)	344.19	29.10
6R-5 (Piece 2)	344.60	29.50
6R-6 (Piece 2)	344.98	31.30
6R-6 (Piece 2)	345.21	32.40
6R-6 (Piece 2)	345.45	32.40
7R-2 (Piece 6)	349.95	7.10
7R-4 (Piece 1)	352.65	7.90
8R-1 (Piece 3)	358.06	8.10
8R-1 (Piece 13)	358.65	8.90
9R-1 (Piece 6)	367.69	7.00
9R-1 (Piece 15)	368.60	7.50
9R-3 (Piece 8)	370.48	5.90
12R-1 (Piece 4)	396.36	7.00
12R-1 (Piece 6)	396.53	6.70
12R-1 (Piece 9)	396.94	6.70
14R-1 (Piece 2)	405.87	7.00
14R-1 (Piece 3)	406.13	7.20
14R-1 (Piece 3)	406.37	6.90
14R-1 (Piece 4)	406.63	7.10
14R-1 (Piece 4)	406.77	6.80
14R-1 (Piece 6)	407.01	6.00
14R-2 (Piece 2)	407.44	7.80
14R-2 (Piece 3)	407.62	7.30
14R-2 (Piece 4)	407.84	6.80
14R-3 (Piece 6)	409.12	8.20
15R-1 (Piece 3)	415.95	6.50
15R-1 (Piece 4)	416.28	6.90
15R-2 (Piece 2)	416.97	6.70
15R-2 (Piece 12)	418.10	7.00
15R-3 (Piece 1)	418.33	6.60
15R-3 (Piece 6)	418.71	8.60
16R-1 (Piece 7)	425.16	5.30
17R-1 (Piece 4)	435.13	8.80
17R-2 (Piece 1)	435.77	15.40
17R-2 (Piece 4)	436.56	18.00
17R-3 (Piece 1)	437.24	28.10
18R-1 (Piece 13)	445.62	21.10
19R-1 (Piece 1)	449.48	27.60
19R-1 (Piece 4)	450.16	28.50
19R-2 (Piece 1)	450.68	36.80
19R-2 (Piece 2)	450.95	35.40
19R-2 (Piece 2)	451.44	36.30
19R-3 (Piece 8)	452.95	26.50
20R-1 (Piece 12)	454.99	17.10
20R-2 (Piece 1)	455.35	25.40
20R-2 (Piece 1)	455.53	26.50
20R-3 (Piece 1)	456.64	20.80
20R-3 (Piece 3)	456.92	25.50
20R-4 (Piece 1)	457.44	23.80
20R-4 (Piece 1)	457.67	27.90
20R-4 (Piece 2)	458.14	20.00
21R-1 (Piece 11)	464.34	23.80
21R-1 (Piece 11)	464.63	25.40
21R-2 (Piece 1)	465.02	20.90
21R-2 (Piece 4)	465.49	25.40
21R-2 (Piece 5)	465.68	26.80
21R-3 (Piece 1)	466.28	27.30
21R-3 (Piece 2)	466.98	28.50
21R-3 (Piece 2)	467.11	31.30
21R-4 (Piece 1)	467.33	30.40
21R-4 (Piece 1)	467.62	29.20
21R-4 (Piece 1)	468.01	27.70
21R-5 (Piece 1)	468.71	21.50
21R-5 (Piece 1)	469.02	21.30
21R-5 (Piece 2)	469.41	22.30
21R-6 (Piece 1)	470.08	23.80
21R-6 (Piece 1)	470.52	24.80
21R-6 (Piece 2)	471.06	19.80
21R-7 (Piece 1)	471.32	23.70
21R-7 (Piece 2)	471.91	23.00
21R-7 (Piece 2)	472.39	28.10
21R-8 (Piece 1)	472.93	29.00
21R-8 (Piece 1)	473.28	29.70
21R-8 (Piece 2)	473.61	33.30
21R-8 (Piece 2)	473.79	32.00
22R-1 (Piece 2)	474.09	37.20
22R-2 (Piece 3)	475.35	34.80
22R-3 (Piece 2)	476.21	31.50
22R-3 (Piece 3)	476.53	25.70
22R-3 (Piece 3)	476.66	24.30
22R-4 (Piece 3)	478.16	35.50
22R-4 (Piece 3)	478.47	32.70
22R-6 (Piece 6)	480.98	34.30
22R-6 (Piece 7)	481.29	32.70
22R-6 (Piece 7)	481.47	29.30
23R-2 (Piece 4)	485.00	15.60
24R-2 (Piece 4)	494.33	13.50
28R-1 (Piece 3)	518.24	29.30
192-1186A-		
30R-2 (Piece 2)	967.83	12.45
30R-2 (Piece 6)	968.43	15.73
31R-1 (Piece 3)	970.26	17.34
31R-3 (Piece 1)	972.89	15.61
31R-3 (Piece 5)	973.33	6.64
31R-3 (Piece 8)	973.55	10.15
31R-4 (Piece 1)	973.97	12.42
31R-4 (Piece 1)	974.23	17.39
32R-1 (Piece 1)	976.93	20.71
32R-1 (Piece 1)	977.24	15.78
32R-2 (Piece 1)	977.77	15.36
32R-2 (Piece 2)	977.97	6.98
32R-2 (Piece 4)	978.45	13.17
32R-3 (Piece 8)	980.18	10.55

Table T4 (continued).

Core, section, piece	Depth (mbsf)	Magnetic susceptibility (10^{-3} SI)
32R-3 (Piece 9)	980.33	11.47
32R-4 (Piece 2)	980.77	15.47
32R-4 (Piece 4)	980.98	14.36
33R-1 (Piece 4)	981.55	14.24
33R-1 (Piece 4)	981.70	17.75
33R-2 (Piece 1)	982.20	32.59
33R-2 (Piece 1)	982.50	30.79
33R-2 (Piece 2)	982.66	29.30
33R-2 (Piece 2)	982.96	29.41
33R-2 (Piece 2)	983.22	28.63
33R-3 (Piece 1)	983.32	30.99
34R-1 (Piece 1)	986.01	35.61
34R-1 (Piece 1)	986.17	32.84
34R-1 (Piece 1)	986.31	31.10
34R-2 (Piece 1)	987.51	31.70
34R-2 (Piece 2)	987.91	34.03
34R-2 (Piece 2)	988.16	34.47
34R-3 (Piece 1)	988.85	30.90
34R-3 (Piece 1)	989.01	33.56
34R-3 (Piece 2)	989.16	33.61
34R-3 (Piece 3)	989.61	31.85
34R-4 (Piece 2)	990.38	24.90
34R-4 (Piece 6)	991.15	18.53
34R-5 (Piece 1)	991.79	21.98
34R-5 (Piece 2)	992.17	23.62
34R-5 (Piece 9)	992.85	22.20
34R-6 (Piece 2)	993.43	20.74
34R-6 (Piece 6)	993.76	17.86
34R-6 (Piece 9)	994.10	18.51
35R-1 (Piece 7)	995.97	19.14
35R-1 (Piece 8)	996.18	19.67
35R-1 (Piece 3)	996.30	19.20
35R-1 (Piece 10)	996.51	22.28
35R-1 (Piece 12)	996.72	15.79
35R-2 (Piece 14)	998.12	14.44
35R-2 (Piece 15)	998.26	10.86
37R-1 (Piece 3)	1015.09	21.28
37R-1 (Piece 3)	1015.46	22.41
37R-1 (Piece 6)	1016.07	18.61
37R-2 (Piece 6)	1016.77	17.64
37R-3 (Piece 1)	1016.96	18.80
37R-3 (Piece 1)	1017.18	20.43
37R-3 (Piece 1)	1017.55	23.98
37R-3 (Piece 1)	1017.81	24.24
38R-1 (Piece 2)	1019.65	38.17
38R-1 (Piece 3)	1019.94	38.20
38R-1 (Piece 3)	1020.12	38.34
38R-1 (Piece 4)	1020.69	34.27
38R-2 (Piece 1)	1021.02	20.01
38R-2 (Piece 2)	1021.56	23.24
38R-2 (Piece 5)	1022.21	20.64
38R-3 (Piece 1)	1022.39	20.30
38R-3 (Piece 3)	1022.83	25.52
38R-3 (Piece 5)	1023.26	29.85
38R-3 (Piece 5)	1023.53	29.30
38R-4 (Piece 1)	1023.90	27.61
38R-4 (Piece 1)	1024.29	25.07
38R-4 (Piece 1)	1024.77	34.12
39R-1 (Piece 1)	1024.46	29.41
39R-1 (Piece 1)	1024.88	34.83
39R-1 (Piece 2)	1025.37	33.54
39R-3 (Piece 3)	1027.88	25.48
39R-3 (Piece 3)	1028.28	27.74
39R-4 (Piece 1)	1028.43	24.56
39R-4 (Piece 4)	1028.98	26.23
39R-4 (Piece 4)	1029.32	28.05
39R-5 (Piece 1)	1029.85	32.64
39R-5 (Piece 1)	1030.05	31.47
39R-5 (Piece 1)	1030.42	31.96
192-1187A-		
2R-2 (Piece 2)	367.14	6.84
2R-2 (Piece 9)	367.68	8.18
3R-1 (Piece 1)	374.58	7.82
3R-1 (Piece 5)	374.91	7.17
3R-1 (Piece 13)	375.50	7.56
3R-1 (Piece 14)	375.89	7.23
3R-2 (Piece 2)	376.20	8.12
3R-2 (Piece 3)	376.55	7.87
3R-2 (Piece 11)	377.37	7.95
3R-3 (Piece 2)	377.59	7.64
3R-3 (Piece 3)	377.81	7.87
3R-3 (Piece 3)	378.01	6.96
3R-3 (Piece 4)	378.31	5.79
3R-3 (Piece 8)	378.77	8.27
3R-4 (Piece 1)	378.98	8.48
3R-4 (Piece 22)	380.31	5.44
3R-5 (Piece 1)	380.55	7.97
3R-5 (Piece 2)	380.72	6.60
3R-5 (Piece 4)	381.19	4.91
3R-5 (Piece 8)	381.28	3.10
3R-5 (Piece 9)	381.44	6.13
3R-5 (Piece 11)	381.58	7.95
4R-1 (Piece 3)	384.32	7.85
4R-1 (Piece 6)	384.81	8.99
4R-1 (Piece 7)	385.01	7.50
4R-2 (Piece 6)	386.01	7.60
4R-2 (Piece 13)	386.72	7.26
4R-2 (Piece 13)	386.98	7.04
4R-3 (Piece 6)	387.60	7.85
4R-3 (Piece 8)	387.97	7.69
4R-3 (Piece 13)	388.49	7.96
4R-4 (Piece 3)	389.03	8.44
4R-4 (Piece 4)	389.30	7.30
4R-5 (Piece 1)	390.02	8.51
4R-5 (Piece 4)	390.39	7.25
4R-5 (Piece 5)	390.77	7.63
4R-6 (Piece 1)	391.54	8.02
4R-6 (Piece 1)	391.66	7.84
4R-6 (Piece 1)	391.75	8.00
5R-1 (Piece 3)	394.14	6.76
5R-1 (Piece 3)	394.30	9.48
5R-1 (Piece 4)	394.54	7.07
5R-1 (Piece 6)	394.98	6.82
5R-2 (Piece 1)	395.27	7.63
5R-2 (Piece 1)	395.55	8.28
5R-2 (Piece 2)	395.91	8.34
5R-2 (Piece 2)	396.24	8.14
5R-2 (Piece 2)	396.44	7.69
5R-3 (Piece 1)	396.73	7.00
5R-3 (Piece 4)	397.36	9.23
5R-3 (Piece 5)	398.04	5.61
5R-4 (Piece 4)	398.73	10.70
5R-4 (Piece 4)	398.90	8.60
5R-4 (Piece 6)	399.51	7.14
5R-5 (Piece 2)	399.74	2.95
5R-5 (Piece 4)	399.98	6.86
5R-5 (Piece 5)	400.20	7.01
5R-5 (Piece 9)	400.70	7.77
5R-6 (Piece 1)	401.28	7.46
5R-6 (Piece 1)	401.43	7.72
5R-6 (Piece 3)	401.93	8.40
5R-6 (Piece 4)	402.18	7.04
5R-7 (Piece 1)	402.68	8.80
5R-7 (Piece 4)	403.29	5.04
5R-7 (Piece 4)	403.39	4.98
5R-8 (Piece 2)	403.90	6.61
6R-1 (Piece 5)	403.75	
6R-1 (Piece 14)	404.48	8.17
6R-2 (Piece 2)	405.86	10.83
6R-3 (Piece 2)	406.20	3.86
6R-3 (Piece 2)	406.45	8.33
6R-3 (Piece 3)	406.72	8.35
6R-3 (Piece 5)	407.01	7.70
6R-3 (Piece 5)	407.25	8.58
6R-4 (Piece 1)	407.82	8.63
6R-4 (Piece 1)	408.04	8.77
6R-5 (Piece 1)	408.47	7.70
6R-5 (Piece 1)	408.71	7.97
6R-5 (Piece 1)	409.03	6.79
6R-5 (Piece 1)	409.27	7.91
6R-6 (Piece 1)	409.86	8.10
6R-6 (Piece 2)	409.99	5.40
6R-6 (Piece 2)	410.09	8.05
6R-6 (Piece 2)	410.38	17.93
6R-7 (Piece 1)	410.89	8.33
6R-7 (Piece 2)	411.17	6.38
6R-7 (Piece 2)	411.51	9.78
7R-1 (Piece 3)	413.26	10.80
7R-1 (Piece 4)	413.45	10.09
7R-1 (Piece 4)	413.64	6.44
7R-1 (Piece 4)	413.97	7.25
7R-1 (Piece 5)	414.34	7.48
7R-2 (Piece 1)	414.71	7.24
7R-2 (Piece 4)	415.18	8.20
7R-2 (Piece 5)	415.44	7.91
7R-3 (Piece 1)	416.01	6.97
7R-3 (Piece 2)	416.52	13.70
7R-3 (Piece 2)	416.81	9.01
7R-4 (Piece 1)	417.09	8.65
7R-4 (Piece 1)	417.25	8.76
7R-4 (Piece 1)	417.34	7.60
7R-4 (Piece 2)	417.48	6.78
7R-4 (Piece 2)	417.75	7.83
7R-4 (Piece 4)	418.01	6.64
7R-5 (Piece 1)	418.44	8.00
7R-5 (Piece 4)	418.98	7.93
7R-5 (Piece 4)	419.11	8.18
7R-6 (Piece 1)	419.46	7.19
7R-6 (Piece 1)	419.76	7.44
7R-6 (Piece 5)	420.23	8.01
7R-7 (Piece 1)	420.65	9.00
7R-7 (Piece 2)	421.01	7.46
7R-7 (Piece 2)	421.26	9.64
8R-1 (Piece 7)	422.96	7.37
8R-1 (Piece 7)	423.05	7.05
8R-1 (Piece 7)	423.23	6.14
8R-2 (Piece 1)	424.12	6.71
8R-2 (Piece 2)	424.43	4.09
8R-2 (Piece 3)	424.63	5.28
8R-2 (Piece 5)	424.94	7.20
8R-3 (Piece 1)	425.51	7.26
8R-3 (Piece 1)	425.77	10.45
8R-3 (Piece 1)	425.94	12.35
8R-3 (Piece 1)	426.13	8.45
8R-3 (Piece 1)	426.27	6.86
8R-3 (Piece 2)	426.51	4.50
8R-3 (Piece 2)	426.70	7.94
8R-4 (Piece 2)	427.06	7.00
8R-4 (Piece 2)	427.20	7.79
8R-4 (Piece 3)	427.68	7.49
8R-4 (Piece 3)	427.97	7.96
8R-5 (Piece 1)	428.32	6.84
8R-5 (Piece 2)	428.59	8.52
8R-5 (Piece 3)	428.87	7.11
8R-5 (Piece 5)	429.19	6.20

Table T4 (continued).

Core, section, piece	Depth (mbsf)	Magnetic susceptibility (10^{-3} SI)
8R-5 (Piece 6)	429.38	17.92
8R-6 (Piece 1)	429.84	6.30
8R-6 (Piece 2)	430.23	7.57
8R-6 (Piece 3)	430.55	11.10
8R-7 (Piece 1)	431.06	9.85
8R-7 (Piece 2)	431.31	15.60
8R-7 (Piece 2)	431.47	7.84
9R-1 (Piece 1)	432.55	7.25
9R-1 (Piece 3)	433.18	6.80
9R-2 (Piece 1)	433.99	7.18
9R-2 (Piece 4)	434.45	7.31
9R-3 (Piece 2)	435.20	2.71
9R-3 (Piece 4)	435.55	7.03
9R-3 (Piece 5)	436.03	16.65
9R-4 (Piece 2)	436.66	14.47
9R-4 (Piece 2)	436.88	13.30
9R-4 (Piece 3)	437.34	15.40
9R-5 (Piece 1)	437.67	6.34
9R-5 (Piece 3)	437.94	5.72
9R-5 (Piece 3)	438.14	13.70
9R-5 (Piece 4)	438.46	10.00
9R-6 (Piece 12)	440.28	7.09
9R-7 (Piece 3)	440.65	6.12
10R-1 (Piece 6)	442.54	6.84
10R-2 (Piece 4)	443.75	5.64
10R-2 (Piece 6)	443.88	5.86
10R-2 (Piece 9)	444.59	6.72
10R-3 (Piece 4)	446.02	5.72
10R-4 (Piece 1)	446.33	6.83
10R-4 (Piece 2)	446.64	7.59
10R-4 (Piece 4)	447.19	7.94
10R-5 (Piece 1)	447.59	12.53
10R-5 (Piece 2)	447.74	8.73
10R-5 (Piece 2)	448.04	6.86
10R-6 (Piece 1)	448.58	8.27
10R-6 (Piece 1)	448.81	6.33
10R-6 (Piece 4)	449.26	11.52
10R-7 (Piece 1)	449.80	15.44
10R-7 (Piece 1)	449.97	16.48
10R-7 (Piece 1)	450.14	5.90
10R-7 (Piece 2)	450.44	5.93
11R-1 (Piece 4)	451.67	6.82
11R-1 (Piece 8)	452.17	4.77
11R-2 (Piece 1)	452.78	7.29
11R-2 (Piece 1)	452.97	9.39
11R-2 (Piece 1)	453.17	5.84
11R-2 (Piece 2)	453.61	7.32
11R-2 (Piece 4)	454.01	7.07
11R-3 (Piece 1)	454.44	8.18
11R-3 (Piece 3)	455.02	8.01
11R-4 (Piece 1)	455.32	8.12
11R-4 (Piece 1)	455.65	8.46
11R-4 (Piece 5)	456.14	9.46
11R-4 (Piece 6)	456.42	14.76
11R-5 (Piece 1)	456.73	9.72
11R-5 (Piece 2)	457.10	13.16
11R-5 (Piece 2)	457.30	6.20
11R-5 (Piece 4)	457.50	6.30
11R-5 (Piece 5)	457.66	8.93
11R-6 (Piece 3)	458.39	13.54
12R-1 (Piece 4)	461.35	12.20
12R-1 (Piece 12)	461.81	8.49
12R-1 (Piece 14)	462.17	7.23
12R-1 (Piece 17)	462.44	8.50
12R-2 (Piece 7)	463.07	8.57
12R-2 (Piece 8)	463.30	9.29
12R-2 (Piece 11)	463.70	10.58
12R-3 (Piece 2)	464.24	19.81
12R-4 (Piece 1)	465.51	14.23
12R-4 (Piece 1)	465.83	12.70
12R-4 (Piece 2)	466.30	18.61
12R-5 (Piece 1)	467.13	22.17
12R-5 (Piece 2)	467.38	17.62
13R-1 (Piece 8)	471.35	10.36
13R-2 (Piece 1)	472.19	13.46
13R-3 (Piece 1)	473.50	7.51
13R-3 (Piece 2)	473.63	7.72
13R-3 (Piece 5)	474.10	9.45
13R-4 (Piece 1)	474.90	18.34
13R-4 (Piece 4)	475.38	18.57
13R-5 (Piece 1)	475.76	6.96
13R-5 (Piece 1)	476.17	7.45
13R-5 (Piece 6)	477.11	7.02
13R-6 (Piece 1)	477.23	7.54
13R-6 (Piece 16)	478.29	7.79
14R-1 (Piece 8)	480.61	7.35
14R-1 (Piece 10)	481.02	8.64
14R-1 (Piece 14)	481.44	8.10
14R-2 (Piece 9)	482.24	9.13
14R-2 (Piece 18)	482.96	7.77
14R-3 (Piece 1)	483.32	7.98
14R-3 (Piece 4)	484.17	7.72
14R-3 (Piece 7)	484.64	8.39
14R-4 (Piece 1)	484.79	7.30
14R-4 (Piece 5)	485.35	6.78
15R-2 (Piece 2)	491.65	6.69
15R-3 (Piece 1)	492.25	10.17
15R-3 (Piece 3)	492.59	12.44
15R-3 (Piece 3)	492.82	11.59
15R-3 (Piece 3)	493.18	11.92
15R-4 (Piece 1)	493.63	8.64
16R-1 (Piece 4)	500.00	7.99
16R-1 (Piece 5)	500.19	7.33
16R-1 (Piece 5)	500.43	6.38
16R-2 (Piece 1)	500.78	7.43
16R-2 (Piece 1)	501.28	7.17
16R-2 (Piece 7)	501.78	8.19
16R-3 (Piece 1)	502.14	6.72
16R-3 (Piece 3)	502.41	9.63
16R-3 (Piece 4)	503.04	7.46
16R-3 (Piece 4)	503.28	7.41
16R-4 (Piece 1)	503.54	7.37
16R-4 (Piece 7)	504.43	7.69
16R-4 (Piece 7)	504.62	7.54
16R-5 (Piece 2)	505.21	6.78
16R-5 (Piece 3)	505.63	7.38

Table T5. Thermal conductivity data for Sites 1183, 1185, 1186, and 1187.

Core, section, interval (cm)	Depth (mbsf)	Thermal conductivity (W/[m·K])
192-1183A-		
54R-5, 54–56	1132.67	1.670
55R-1, 50–52	1137.00	1.692
56R-2, 8–10	1147.53	1.729
57R-1, 83–85	1151.83	1.995
58R-2, 30–32	1157.52	1.711
59R-1, 56–58	1161.16	1.947
59R-2, 64–66	1162.69	1.856
60R-1, 144–146	1167.94	1.765
60R-2, 10–12	1168.10	1.757
61R-1, 76–78	1176.90	1.784
61R-2, 7–9	1177.60	1.798
62R-1, 60–62	1181.60	1.944
62R-3, 33–35	1184.20	1.833
63R-1, 43–45	1186.20	1.652
64R-2, 75–77	1192.80	2.004
65R-1, 90–92	1196.30	1.835
65R-2, 68–70	1197.50	1.792
65R-3, 25–27	1198.40	1.828
66R-1, 98–100	1201.10	1.446
66R-2, 86–88	1202.40	1.786
66R-3, 54–56	1203.50	1.754
67R-1, 21–23	1205.10	1.729
67R-3, 113–115	1209.00	1.829
68R-1, 30–32	1210.00	1.746
192-1185A-		
2R-1, 30–32	250.90	1.314
6R-1, 90–92	290.00	1.332
7R-1, 140–142	300.20	1.302
7R-1, 141–143	300.21	1.308
8R-2, 90–92	310.80	1.797
9R-2, 50–52	319.00	1.711
10R-2, 75–77	324.73	1.604
11R-1, 45–47	328.15	1.790
192-1185B-		
3R-2, 69–71	317.80	1.424
3R-2, 99–101	318.10	1.452
4R-3, 49–51	321.67	1.736
4R-6, 29–31	325.51	1.708
5R-1, 26–28	329.07	1.750
5R-7, 137–139	337.96	1.638
6R-2, 34–36	339.82	1.936
6R-6, 74–76	345.55	1.959
7R-1, 89–91	349.00	1.580
8R-1, 29–31	358.00	1.644
9R-2, 114–116	369.82	1.708
10R-2, 7–9	378.44	1.735
11R-1, 102–104	387.53	1.883
12R-1, 39–41	396.50	1.760
13R-1, 19–21	400.40	1.369
14R-2, 109–111	408.30	1.592
15R-1, 64–66	415.95	1.871
15R-2, 64–66	417.45	1.641
16R-1, 114–116	426.05	1.824
17R-3, 9–11	437.23	1.778
17R-3, 39–41	437.51	1.785
18R-1, 129–131	445.60	1.728
19R-1, 139–141	450.51	1.849
20R-2, 70–72	455.86	1.790
21R-3, 99–101	466.85	1.807
21R-8, 66–68	473.31	1.841
22R-3, 59–61	476.56	1.883
22R-5, 94–96	479.78	1.860
23R-2, 89–91	485.20	1.770
24R-2, 110–112	495.10	1.725
28R-1, 29–31	517.91	1.841
28R-1, 52–54	518.13	1.856
192-1186A-		
30R-1, 60–62	967.00	1.749
31R-1, 40–42	970.40	1.781
32R-4, 50–52	981.16	1.738
33R-2, 7–9	982.12	1.776
34R-3, 86–88	989.55	1.807
35R-1, 20–22	995.70	1.754
37R-3, 10–12	1016.90	1.804
38R-1, 40–42	1019.80	1.885
39R-1, 110–112	1025.50	1.947
39R-4, 40–42	1028.80	1.796
192-1187A-		
2R-3, 5–7	368.19	1.621
3R-3, 35–37	377.79	1.680
4R-2, 44–46	386.13	1.656
4R-5, 30–32	390.16	1.759
5R-2, 100–102	396.18	1.756
5R-6, 110–112	402.21	1.810
5R-6, 111–113	402.22	1.724
6R-2, 125–127	405.88	1.623
6R-6, 65–67	410.18	1.827
7R-3, 105–107	416.78	1.649
7R-3, 106–108	416.79	1.725
8R-1, 66–68	423.26	1.666
8R-3, 43–45	425.77	1.685
8R-6, 16–18	429.66	1.830
9R-3, 70–72	435.79	1.882
9R-6, 70–72	439.67	1.704
10R-4, 20–22	446.32	1.726
10R-7, 22–24	449.81	1.790
10R-7, 23–25	449.82	1.868
11R-2, 30–32	453.00	1.770
11R-5, 50–52	457.10	1.802
12R-5, 35349	466.65	1.838
13R-1, 60–62	471.30	1.706
13R-4, 25–27	474.92	1.790
14R-2, 45–47	482.25	1.581
14R-4, 76–78	485.44	1.769
14R-4, 77–79	485.45	1.674
15R-2, 88–90	491.73	1.691
15R-4, 35–37	493.82	1.812
15R-4, 36–38	493.83	1.801
16R-2, 55–57	501.19	1.693
16R-5, 80–82	505.62	1.698